Materials Science and Engineering R 70 (2010) 169–187

Contents lists available at ScienceDirect

Materials Science and Engineering R

journal homepage: www.elsevier.com/locate/mser

Formation and structural transition of molecular self-assembly on solid surface investigated by scanning tunneling microscopy

Dong Wang, Li-Jun Wan *, Chun-Li Bai **

Institute of Chemistry, Chinese Academy of Sciences, Beijing 100190, China

ARTICLE INFO

Article history:
Available online 30 June 2010

Keywords:
Self-assembly
Scanning tunneling microscopy
Surface and interface

ABSTRACT

The spontaneous formation of ordered self-assembly on solid supports is not only an intriguing subject for fundamental surface science study, but also closely related to many emerging technologically important applications, especially in the field of nanotechnology. With the help of scanning tunneling microscopy (STM) at sub-molecular resolution, the detailed structural information within the self-assembled monolayers can be obtained, which allows us to have an insight into how the interplay between the intermolecular weak interactions and the substrate–molecule interactions governs the formation of molecular self-assembly. In this review, the structural transition of self-assembly in response to the subtle differences in the molecular structures and/or the environment change will be presented. The fundamental understanding about the driving force controlling the assembly process promotes the development of various means to tune the structural transition of supramolecular assembly on solid surfaces and fabricate the sophisticated architectures. Finally, some future directions in the field are outlined.

Contents

* Corresponding author. Tel.: +86 10 6255 8934; fax: +86 10 6255 8934.
** Co-corresponding author.
E-mail address: wanlijun@iccas.ac.cn (L.-J. Wan).

0927-796X/$ – see front matter © 2010 Elsevier B.V. All rights reserved.
doi:10.1016/j.mser.2010.06.016

1. Introduction

Nanoscience and nanotechnology are the study of materials, devices, and systems through the control of matter on the nanometer-scale. Its essence is the ability to work at these levels to generate nanostructures exhibiting novel physical, chemical, and biological properties and phenomena. The aim of nanoscience and nanotechnology is to exploit these properties and efficiently manufacture and employ the nanostructures. The control of matter at nanoscale has already shown a huge impact on the development of scientific disciplines as diverse as physics, chemistry, materials science, biology, medicine, engineering, and computer science.

The fabrication of well-defined nanostructures on solid surfaces is one active research field in nanoscience and nanotechnology [1,2]. Two different strategies are generally used to obtain well-defined nanostructures. In the "top-down" approach, which is represented by photolithography, the desired nanostructures are fabricated through cutting, milling of large-scale objects into nanometer-scale. On the other hand, the "bottom-up" approach strives for constructing nanostructures from the basic "building blocks" such as atoms, molecules, and other nano-objects. The main advantages of the bottom-up approach include high efficiency, fast and simple operation process, and high preciseness. The key challenge of the bottom-up approach, however, lies on finding a proper way to handle and control the nano-objects into the desired architectures. Self-assembly is the most promising and representative bottom-up approach to build up nanostructures. In fact, nature has adopted the similar bottom-up strategy to build up sophisticated yet functional architectures via self-assembly. One typical example is the double helix structure of deoxyribonucleic acid (DNA), which is formed through the hydrogen bonding driven self-assembly of the DNA base pairs. Mimicking the self-assembly process in nature to construct supramolecular nanostructures on solid supports is not only an intriguing subject for fundamental surface science study, but also closely related to many emerging technologically important applications, especially in the field of molecular electronics. In this regards, understanding the underlying mechanism for the formation of self-assembled nanostructures is a key physical chemistry problem towards the controllable fabrication of surface nanostructures with desired properties and functions.

The invention of scanning tunneling microscopy (STM) [3] provides us a powerful tool to study the surface self-assembly [4]. With the help of STM at sub-molecular resolution, the detailed structural information within the self-assembled monolayers (SAM) can be obtained, which allows us to have an insight into how the interplay between the intermolecular weak interactions and substrate–molecule interactions governs the formation of molecular self-assembly [5–8]. Understanding the weak interactions controlling the assembly of molecules on solid surface provides us a good opportunity to fabricate the sophisticated architectures, which would potentially be used in single molecular devices, molecular electronics, surface nanopatterning, among others.

In this review, we will describe the latest progress in the field of surface self-assembly. Due to the space limitation, many interesting results from ultrahigh vacuum environment are excluded here, although those results have supplied important contributions towards understanding the self-assembly process [9,10]. The self-assembly of alkanes and alkane derivatives will be introduced first as model systems to illustrate the important role of weak interactions in the self-assembly process. The main focus will be on the structural transition of self-assembly in response to the subtle differences in the molecular structures and/or the environment change. These results not only provide us fundamental knowledge about the driving force controlling the assembly process, but also give us great opportunities to fabricate the sophisticated architectures via a bottom-up approach. Finally, some future directions in the field are outlined.

2. Self-assembly of alkane derivatives

2.1. Physisorbed alkane derivatives

Alkanes and their derivatives [$CH_3(CH_2)_nX$, X = CH_3, OH, COOH, Cl, Br, I, NH_2, SH] have been employed as model systems to exploit how the intermolecular interactions and substrate–molecule interactions affect the self-assembled structures [11]. The alkane molecules are saturated linear molecules with carbon atoms arranged in a zigzag structure. The length of a C–C–C zigzag period is 0.251 nm. n-Alkanes can adsorb on solid surfaces such as highly ordered pyrolytic graphite (HOPG) [12], MoS_2 [13], Au(1 1 1) [14], Pt(1 1 1) [15], Ag(1 1 1) [16] and their structures have been studied by various techniques including low-energy electron diffraction (LEED), neutron diffraction, X-ray scattering, infrared (IR), and STM. Among these characterization tools, STM provides the direct real space evidence for the self-assembly structure and the registry between adlayer and substrate at atomic resolution. Fig. 1a shows a typical STM image of $C_{18}H_{38}$ on HOPG [11]. The molecules pack side-by-side in adjacent lamellas with an angle of 90° between the

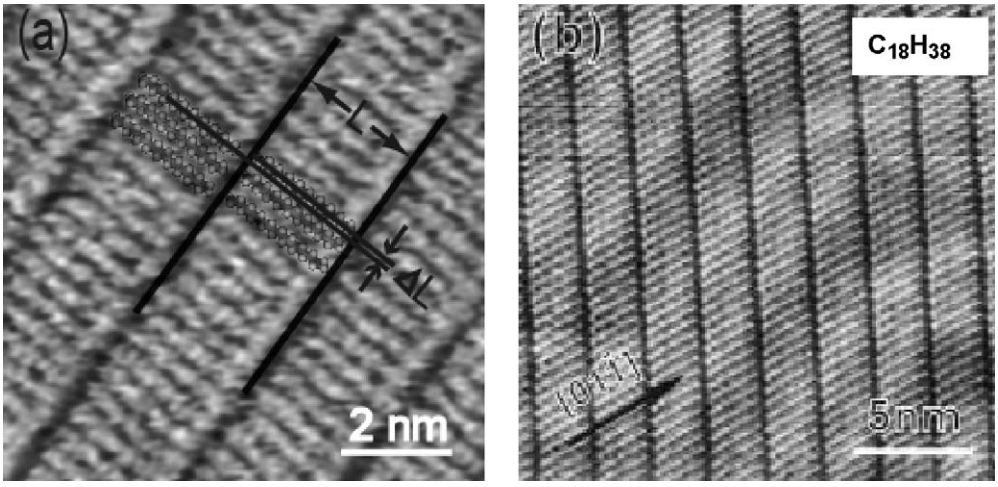

Fig. 1. STM images of $C_{18}H_{38}$ on HOPG [11] (a) and on reconstructed Au(1 1 1) [23] (b).

molecular alkyl chain axis and the molecular alignment row direction. The length of each row extracted from the image is *ca.* 2.42 nm, close to the theoretical length of a fully extended $C_{18}H_{38}$ [17,18]. $C_{13}H_{28}$ molecule is found to be the shortest alkane capable of forming ordered adlayer on HOPG. For the alkanes with shorter alkyl chains, the molecules become too mobile to form ordered monolayer on substrate at room temperature due to the thermal motion. Similar lamella structures are observed for all the alkanes up to $C_{50}H_{102}$ [19]. Theoretical calculation indicates the adsorption energy per CH_2 on HOPG is −12.1 and −10.4 kJ/mol in the flat and vertical orientation, respectively [20]. Therefore, every methylene in alkane molecules is proposed to locate in a carbon hexagonal ring of HOPG with a flat-lying configuration, according to Groszek model [21,22]. In this arrangement, the van der Waals interactions between the alkane molecules and substrate can be maximized.

On the basis of the self-assembled structure from STM result, a correlation between the width of the alkane lamella and the number of carbon atoms in an alkyl chain exists. The relation can be described as:

$$L = \frac{n+2}{2} \times 0.246(nm)$$

Here, L is the width of a lamella formed by alkane molecules and n is the number of carbon atoms in an alkyl chain. 0.246 (nm) corresponds to the periodicity of HOPG lattice [18].

The importance of substrate–molecule interaction in a self-assembly process can be further exemplified from the adsorption of normal alkanes with different carbon chain lengths (n = 14–38) on Au(1 1 1) surface [23–28]. As can be seen from Fig. 1b, an ordered alkane monolayer is only found on the reconstructed Au(1 1 1) surface. The alkane molecules adopt a flat-lying configuration and pack side-by-side to form a lamellar structure. Alkane molecules adsorb along the $[0\,1\,\bar{1}]$ or $[\bar{1}\,0\,1]$ directions of the reconstructed Au(1 1 1) surface. The intermolecular distance along the molecular lamella is measured to be 0.48 nm, which matches well with the distance in the bulk alkane crystal. Therefore, the self-assembled alkane monolayers are commensurate with the reconstructed Au(1 1 1) surface to optimize both adsorbate–adsorbate interactions and adsorbate–substrate interactions. In contrast, the unconstructed Au(1 1 1) surface has a lattice constant of 0.50 nm along the $[1\,\bar{2}\,1]$ direction, and thus no effective self-assembly process could be induced. A length dependent evolution of the tilted angle between the lamella and the molecule backbone is observed. At room temperature (25 °C), tilted lamellae form if $n < 22$; tilted and perpendicular lamellae coexist for $36 > n > 22$; and perpendicular lamellae prevail for $n > 38$. The observed lamellar structures are determined by a combined effect of the adsorbate–adsorbate interactions and the adsorbate–substrate interactions.

The self-assembly of alkane derivatives with different functional groups on HOPG, Au(1 1 1), MoS_2, and other surfaces has been intensively investigated by STM [29–32]. Fig. 2 summaries the structural models for the alkane and several alkane derivaties with 18 and 19 carbon alkyl chains on HOPG surface. In general, these molecules self-assemble into lamella structures on surface. The alkyl backbone lies on the HOPG with molecular axis along the

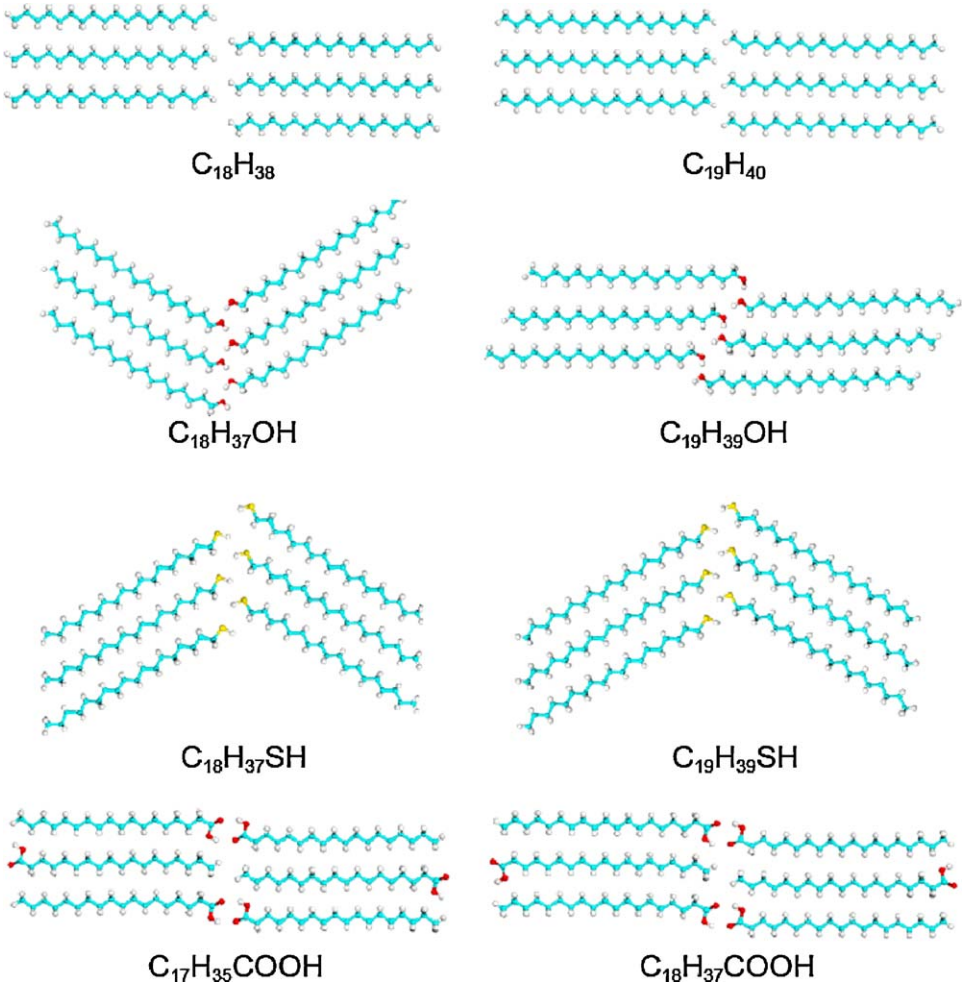

Fig. 2. Structural models for the adlayers of alkanes and alkane derivatives with 18 and 19 carbon atoms on HOPG surface.

⟨1 1 0⟩ direction of the HOPG surface, which is very similar to the molecular configuration of alkanes on surfaces. The effect of the intermolecular interactions between the functional groups can be recognized from the molecular configuration in adjacent lamella and the angle between the molecular axis and the lamellar direction. Hydrogen bonding and van der Waals force play important roles in the formation of ordered self-assembly of alkyl molecules. For the molecules with no hydrogen bonding ability, such as alkanes, the alkyl chains adsorb on HOPG surface with an angle of 90° between the molecular axis and the lamella direction, which can maximize the contact area between molecules in adjacent lamella and thus maximize the intermolecular van der Waals force. For the alkane derivatives that can form hydrogen bonding, the angle between the molecular axis and the direction of lamella alignment is 60° or 90° [11,12,33–35]. Typically, they adopt a head-to-head configuration due to the existence of intermolecular hydrogen bonding. Alkane alcohol molecules show both herringbone and tilted packing in the adlayer, which are verified theoretically to be thermodynamic stable configurations [36]. In both arrangements, there are two intermolecular hydrogen bondings for each hydroxyl group with the adjacent hydroxyl groups, one within the same lamella and the other at the adjacent lamella. For fatty acid, two molecules form a dimer as a basic structural component in the adlayer through intermolecular hydrogen bonding [37–40]. The adjacent molecules along the molecular lamella axis arrange alternately due to large size of carboxylic acid groups. The molecular axis is perpendicular to the lamellar direction. The dipole–dipole interaction is important in forming the self-assembly of alkyl halides [41]. The angle between the molecular axis and the direction of lamella alignment is 90°. There are two types of self-assemblies in the alkyl thiol adlayers: parallel and V-type structures. Considering the relative weak nature of hydrogen bonding between thiols [36,42], hydrogen bonding is not always dominant for the self-assembling process. For $C_{18}H_{37}SH$ and $C_{19}H_{39}SH$ adlayers, V-type structures similar to that of $C_{18}H_{37}OH$ are observed [11,43]. The directionality of the S···H–S bond results in an angle of 60° between the molecular axis and the lamella alignment direction. With the increase of alkyl chain length to $C_{22}H_{45}SH$, the adsorbate–graphite and the alkyl–alkyl interactions control the adsorption process, the linear structure is formed with both "head-to-head" and "head-to-tail" arrangements [41].

One interesting observation in the self-assembly of alkane derivatives is the odd-even effect, i.e. dependence of the self-assembled structure on the number of carbon atoms in alkyl chain [44]. For example, the self-assembly of $C_{19}H_{39}Br$ is different from that of $C_{18}H_{37}Br$ and $C_{22}H_{45}Br$ [41]. It is observed that the bromine atoms in $C_{19}H_{39}Br$ appear in "bright" contrast in STM images, while both "dark" and "bright" contrasts are observed for $C_{18}H_{37}Br$ and $C_{22}H_{45}Br$. The angle formed between the molecular axis and the lamella direction is 60° for $C_{19}H_{39}Br$ and 90° for $C_{18}H_{37}Br$. Only "head-to-head" configuration is observed for $C_{18}H_{37}Br$ and $C_{22}H_{45}Br$. Both "head-to-head" and "head-to-tail" configurations exist in $C_{19}H_{39}Br$ assembly. The odd-even effect is also observed for the self-assembly of fatty acids. The self-assembly of $C_{17}H_{35}COOH$ is homochiral, while the self-assembly of $C_{18}H_{37}COOH$ is racemic. The odd-even effect is an elegant example of how subtle difference in chemical structure affects the self-assembly structures [44].

2.2. Chemisorbed SAM of thiols

The chemical adsorption and assembly of alkanethiols is widely used to modify the metal substrates, such as Au, Ag, Pt, and et al. [45–47]. The SAMs are formed by simply dipping a well-defined metal substrate into a dilute solution of alkanethiol for typically 12–24 h. The assembly structure of n-alkanethiols on Au(1 1 1) has been intensively investigated by STM, X-ray diffraction, infrared spectrometry, and many other characterization techniques [48,49]. The adsorption of thiols on Au(1 1 1) results in the lift of surface construction and the formation of local islands and etch pits on the surface. The highly ordered adlayer of the high-coverage thiol phases on Au(1 1 1) is generally accepted to be based on a $(\sqrt{3} \times \sqrt{3})R30^\circ$ overlayer. The adlayer is more accurately described as a $c(4 \times 2)$ superlattice to account for the azimuth of alkyl chains in the SAM. The chemical nature of SAMs is generally accepted as thiolate overlayers with molecules chemisorbed on the gold surface through Au–S bonds. The driving force for the thiolate SAM formation can be ascribed to the strong Au–S bond and the van der Waals interactions between closely packed alkyl chains. The formation of thiolate SAMs is compatible with a variety of functional groups. Therefore, the well-defined SAMs with terminal functional groups, such as carboxylic acid, hydroxyl, ester, halogen, can be prepared by using α,ω-thiols with the desired secondary functional groups as precursors. The thiolate SAMs on metal substrates have been widely applied in a broad range of fields, such as nanomaterials synthesis, nanoelectronics, nanobiology, lithography, among others [50,51]. The detailed discussion of the application of thiolate SAMs is beyond the scope of this review. The readers are referred to several comprehensive reviews for the detailed information about the structure and application of alkanethiol SAMs [52,53].

3. Structural transition of self-assembly

One important prerequisite to apply the self-assembly technique in the "bottom-up" strategy for nanofabrication is to precisely control the structure of 2D molecular assemblies [5]. The study of the structural transition of SAMs on solid surfaces is not only of great importance to understand the self-assembly process, but also provides us valuable information about how to control the molecular nanostructures. The common methods to change the structures of self-assembly include (a) modifying the molecular chemical structures; (b) changing the experiment conditions, such as concentration, solvent, temperature, substrate, etc.; (c) applying external stimuli such as light irradiation, heating, chemical treatment, or electric fields.

3.1. Chemical structure modification

The understanding of the underlying driving force for the molecular self-assembly process provides us basic knowledge for controlling the molecular nanostructure. In fact, the subtle chemical structure difference always brings significant structural transition, which highlights the complexity of surface self-assembly on one hand, and provides us the ability to finely tune the molecular nanostructure on the other hand.

It is well known that the alkane and alkane derivatives can form stable SAMs on HOPG surface through the strong van der Waals interaction. The stabilizing effect of linear alkanes has been utilized to achieve very high stability in the adsorption and assembly of planar organic molecules on HOPG [54–58]. This strategy can be demonstrated by the formation of highly ordered stable SAM using peripherally alkylated phthalocyanines and porphyrins [59,60]. Immobilizing functional organic molecules, such as phthalocyanines and porphyrins, onto the solid substrates is an important prerequisite for the application of these materials in molecular devices. Even though they are known to lie flat on surfaces, their low diffusion barrier makes it difficult to study their electronic properties. By introducing peripheral alkyl chains to the molecule core, however, the extra stability is gained through alkyl/HOPG interaction, while the electronic property of the molecule is preserved. Observations using STM reveal that the copper(II)

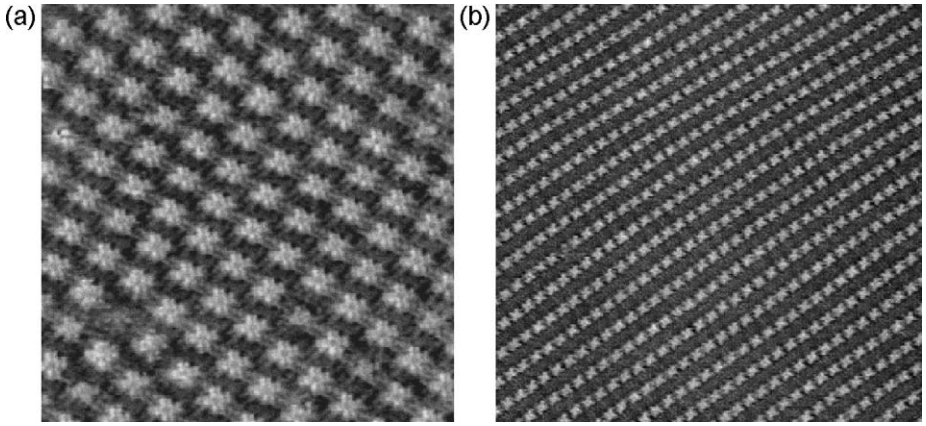

Fig. 3. STM images of alkoxyl-substituted phthalocyanine (a) and porphyrin (b) on HOPG surface [59].

octaalkoxyl-substituted phthalocyanine molecules form a large, uniform molecular array with domain size ranging from tens to hundreds of nanometers, as shown in Fig. 3a. It can be seen that the phthalocyanine molecules form the ordered hexagonal two-dimensional arrays. The phthalocyanine core appears as bright spots with characteristic four-fold symmetry, consistent with its molecular structure. The shaded zigzag lines interconnecting the bright regions correspond to the long alkyl substituents, which are interdigitated to maximize the van der Waals interactions. The observation clearly indicates that the contributions from phthalocyanine molecules dominate the overall contrast, as expected from theoretical calculations. The alkylation strategy could be expanded to other molecular systems. Fig. 3b shows the STM observation of tetra-alkyloxy substituted porphyrin. The large, uniform domains indicate high stability of the assembly. Porphyrins are aligned side-by-side into a lamellar structure, and separated by the interdigitated alkane chains. This result indicates that the assembly formation is directly affected by the 2D crystallization of alkyl chains. Changing the length of alkyloxy substitution chains provides a feasible way to tune the inter-porphyrin distance in the assembly [61].

The successful application of alkylation strategy to construct ordered self-assembly of functional organic molecules encourages us to study the effect of the alkyl chain length on molecular nanostructures. Hexakisalkoxy-substituted triphenylenes with n carbon side chains (Tn) has been studied by several groups to explore the alkyl chain length effect. Rabe and coworkers found T7 molecules keep three-fold symmetry in the assembly, while in T16 all alkyl chains are oriented preferentially parallel to each other [62]. Charra and Cousty studied the self-assembly of T5, T7, T9, and T11 on HOPG [63]. They reported that a chiral ordering transition appears when the number of the methylene units is above nine. Wu and coworkers synthesized a series of Tn derivatives and studied their self-assembly behavior on HOPG [64]. Fig. 4a presents a STM image of a submonolayer assembly of T12. Each molecule can be resolved as a bright spot, which corresponds to the conjugated core, and the shaded linear alkyl substituents. Every seven molecules form an approximate hexagon, with the seventh molecule in the center. The central molecule of a hexagon has a six-fold symmetry, while the molecules located at the corners of the hexagon have three-fold symmetry. With the two additional methylene units on the alkyl substituents (T14), the arrangement of the molecule changes drastically. A characteristic dimer structure is persistent over a large area, as shown in Fig. 4b. The carbon chains of the molecule are divided into two oriented groups, which leads to the loss of the original molecular symmetry. The triphenylene cores are antiparallel to each other within a dimer. The molecular arrangement of T16 changes again. It can be seen from Fig. 4c that the molecules form a well-ordered arrangement with all the alkyl groups parallel to each other, in order to form a tightly packed structure. The neighboring molecules orient in an antiparallel way along the transverse direction of alkyl chains. When the number of the methylene units reaches eighteen (T18) and twenty (T20), the intermolecular spacing within the triphenylene arrays becomes less uniform than that in T16. Fig. 4d is a representative high-resolution image of T20 adlayer. It can be seen that the aromatic cores are no longer uniformly spaced along the array, but rather display a sporadic spacing distribution. The structure evolution of Tn self-assembly can be understood by considering competing contribution from local 2D crystallization of the alkyl chains and the steric hindrance of core molecules. The local crystallization of the alkyl moieties results in highly parallel ordering of linear alkanes regardless of core molecule symmetries, while the steric hindrance of core molecules would favor antiparallel molecular orientations. The outcome of the molecular assembly is determined by the balanced effect of steric interaction and frustrated 2D alkane lamellae.

The structure evolution of the self-assemblies of a series of graphene molecules, hexafluorotribenzo[a,g,m]coronene modified with *n*-carbon alkyl chains (n = 4, 6, 8, 12, *ab.* FTBC-Cn) on HOPG has been investigated [65]. Fig. 5a is a typical high-resolution STM image of FTBC-C4 adlayer. Each molecule appears as a set of three bright spots in a triangular shape, consistent with the calculated lowest unoccupied molecular orbital (LUMO) of FTBC-C4 as shown in the inset of Fig. 5a. Two alternating molecular rows with different contrasts are clearly seen. FTBC-C4 molecules can take two different orientations on HOPG surfaces, i.e., "down" with alkyl chains in contact with HOPG and "up" with conjugated core in contact with substrate. The contrast difference of molecules originates from the different adsorption conformation, which is verified by DFT simulation. The increase of two more methylenes in the alkyl substituents results in the formation of a honeycomb structure for FTBC-C6, as shown in Fig. 5b. Each honeycomb unit is composed of six bright molecules at the corner with a dark depression at the center. The molecular models are depicted and superimposed on the image. FTBC-C8 forms a similar honeycomb assembly. With increase of the alkyl chain length to 12 carbons, van der Waals interaction dominates the self-assembly formation. The adlayer of FTBC-C12 is composed of two distinct structures, lamellar and pseudo-honeycomb structures, as shown in Fig. 5c and d, respectively. The common feature of these two structures is that the alkyl chains interdigitate each other to stabilize the molecular assembly. From the results of scanning tunneling spectroscopy (STS) measurement, it is found that the electronic property of the featured graphene molecules is preserved when they are adsorbed on solid surface. Therefore, the nanostructures of

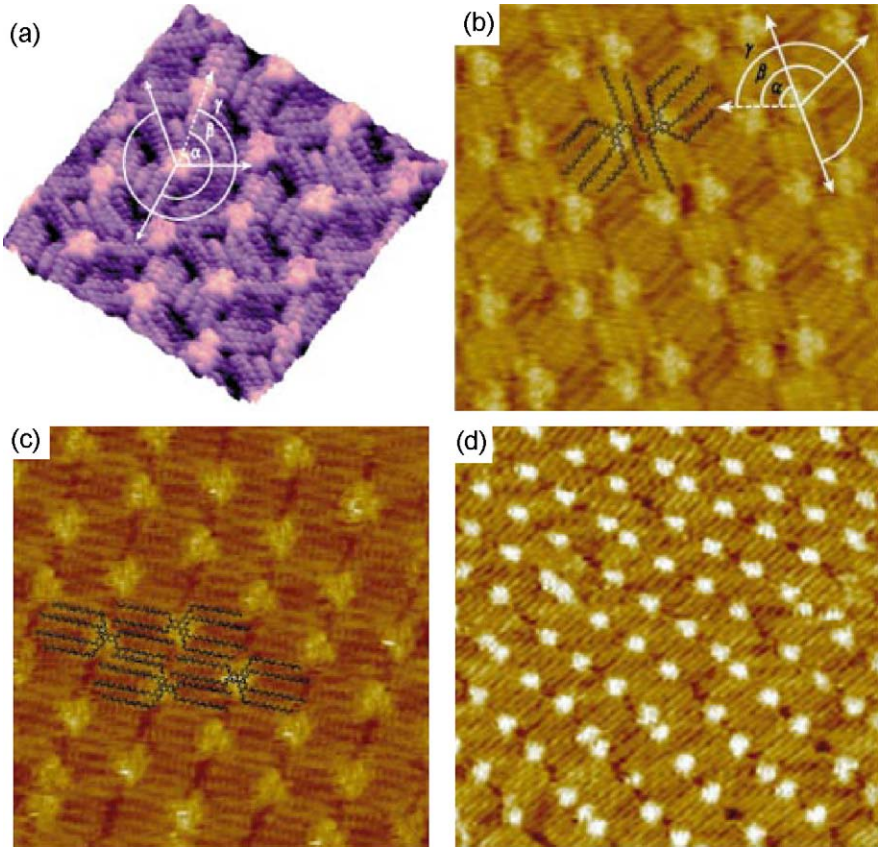

Fig. 4. STM image of the self-assembly of T12 (a), T14 (b), T16 (c), and T20 (d) on HOPG surface [64].

functional molecules can be tuned by attaching periphery alkyl chains without interfering with their physical chemistry properties.

3.2. Effect of substrates

It is well known that substrate can affect the self-assembly of adsorbates [66,67]. The substrate–adsorbates interactions exerted by different substrates can significantly change the molecular self-assembly process. For example, naphthalene can form an ordered $3\sqrt{3} \times 3\sqrt{3}$ structure on Rh(1 1 1), whereas a disordered adlayer is observed on Pt(1 1 1) [68]. It is proposed that the naphthalene cannot move freely on Pt(1 1 1) to form ordered adlayer due to the strong interaction between π electrons and metal surface.

Gong and coworkers found that a supramolecular metallacyclic rectangle adopted different adsorption configuration on HOPG and Au(1 1 1) surfaces [69]. Fig. 6a shows a high-resolution STM image of the adlayer on HOPG. The molecules appear as bright lines and stack into a lamella structure along direction b on HOPG. From the periodicity of the molecular self-assembly, a unit cell with parameters of $a = 4.0 \pm 0.2$ nm (in the A direction), $b = 1.0 \pm 0.2$ nm (in the *B*-direction), and an angle of $90 \pm 2^\circ$ can be determined. In the proposed structural model, the long edge of the rectangle stands on the surface, forming a 2D molecular network. The supramolecular rectangle shows a different assembly structure on Au(1 1 1), as shown in Fig. 6b. Bright rows of rectangles are observed along ⟨1 1 0⟩ direction of Au(1 1 1) substrate. The molecule appears as a rectangle with dark depressions in the center in STM image, as shown by the superimposed molecular models in Fig. 6b. The molecular size of the rectangle was determined to be 3.0 ± 0.2 by 1.1 ± 0.2 nm, consistent with the size of the rectangle determined from the X-ray crystallographic data. The intermolecular distance along B-direction is measured to be ca. 2.0 nm. In the proposed structural model, each molecule preserves its rectangular shape with the face of the rectangle lying flat on the Au(1 1 1) surface, forming a well-ordered self-organized pattern.

Kudernac and coworkers investigated the polymorphism of Schiff base derivatives in the self-assembly process [70]. Whereas a similar columnar structure of PHB [4-(dodecyloxy)-N-(4-dodecylphenyl)-2-hydroxybenzaldimine], a Schiff base substituted by alkyl side chains, is observed on HOPG, MoS_2, and alkane modified HOPG surfaces, both the columnar structure and a new dimer structure are obtained on a Au(1 1 1) surface. Theoretical and experimental results demonstrate that molecule/substrate interactions modify the chemical nature of the molecule by charge transfer with the metal, which in turn modify molecule/molecule interactions, and result in the observation of polymorphism on Au(1 1 1). In the dimer packing observed on Au(1 1 1), the increased equilibrium distance between pairs of PHB compensates for the stronger molecule/molecule repulsive interactions.

3.3. Solvent effect

Solvent is an important player in the solid/liquid interface self-assembly process [71]. The solvent molecules can modulate the adlayer structure by tuning the interface environment [72], such as polarity, solubility, viscosity, or forming co-adsorption with adsorbates [39,73] through hydrogen bonding and van der Waals interactions.

The self-assembly of trimesic acid (TMA) on a HOPG substrate results in the formation of two different open, loosely packed, two-dimensional hydrogen bond networks, e.g. "chickenwire" and "flower" structures. These two polymorphs differ in their molecular packing density and hydrogen bonding schemes. The

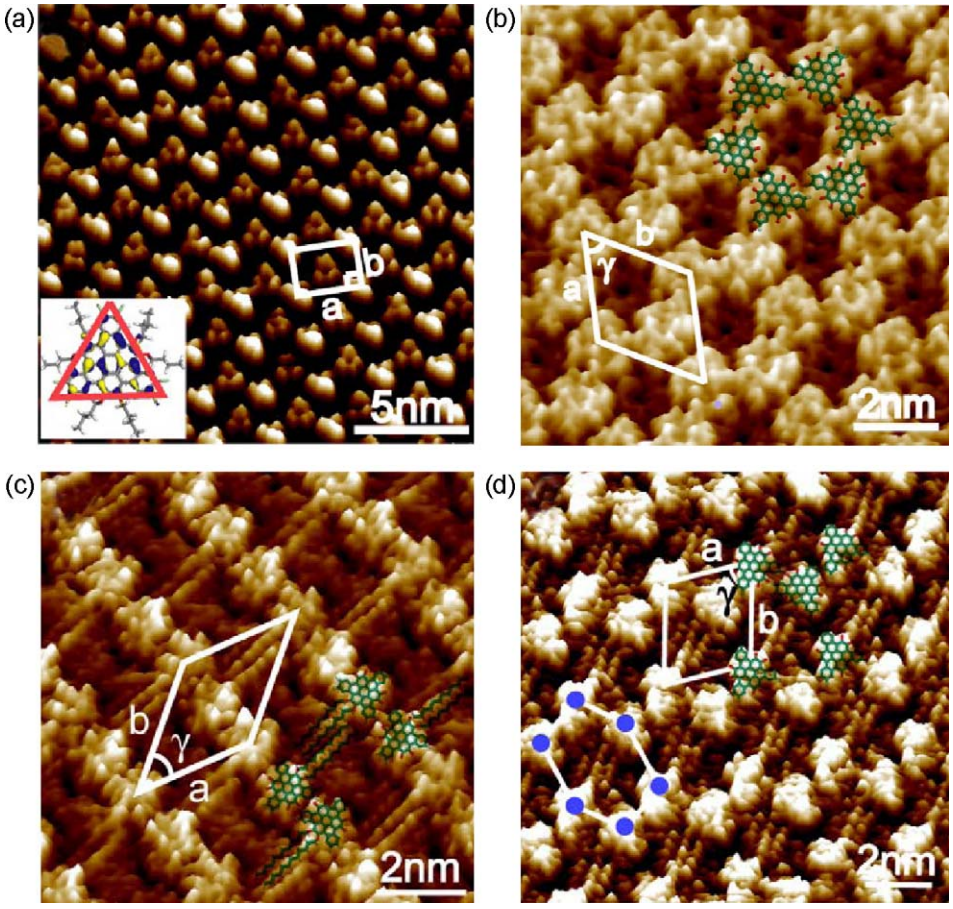

Fig. 5. (a) Self-assembly of FTBC-C4 on HOPG with an alternate "up-down" adsorption configuration. (b) Self-assembly of FTBC-C6 on HOPG with a honeycomb structure. (c and d) Self-assembly of FTBC-C12 with lamellar structure and pseudo-honeycomb structure [65].

selective formation of either structure can be tuned by choosing the proper solvents [74,75]. The longer-chain solvents favored the formation of the chickenwire polymorph structure on the surface. 1,3,5-Benzenetribenzoic acid, which has a similar structure to TMA, also shows solvent-dependent polymorphic structures on HOPG [75]. The solvent polarity is proposed to explain the observed solvent effect.

Chen et al. reported the solvent effect on chiral assembly of 1,4-di [4-N-(trihydroxymethyl)methyl carbamoylphenyl]-2,5-didodecyloxybenzene (DTCD) molecules on HOPG surface [76]. Fig. 7a and b shows high-resolution STM images of the DTCD adlayer prepared from THF. Each bright rod in the STM images is attributed to a DTCD molecule. Four DTCD molecules congregate head-to-head in a helix fashion and give a windmill-shaped tetramer, which is the basic unit of the ordered 2D pattern. The rotational direction of the windmill-shaped tetramer determines the chirality of the adlayer. For example, the anti-clockwise windmills are seen in Fig. 7a and the clockwise windills are seen in Fig. 7b. Therefore, the supramolecular assemblies in Fig. 7a and b possess opposite surface chirality. The intermolecular hydrogen bonding is proposed as the driving force for the formation of homochiral structures. A similar chiral assembly is observed when phenyloctane is used as solvent. In contrast, a heterochiral assembly is formed when the adlayer is prepared from 1-octanol. As shown in Fig. 7c, DTCD molecules form a well-ordered lamella structure. The molecular dimer is the essential subunit of the adlayer. They adsorb on the HOPG surface head-to-head and give birth to lamellar arrangement. Interestingly, two chiral species of the molecular dimer, designated as λ and δ in Fig. 7c, can be found in the adlayer. This is understandable since the molecular dimer can land on the surface with either face uppermost, just like a prochiral molecule [77]. The molecular dimers with the same chirality organize head-to-tail and form a molecular lamella. The chirality of the molecular dimers changes alternatively in the neighboring lamella. Therefore, a racemic supramolecular assembly is obtained. Careful inspection of the heterochiral pattern shows the existence of the co-adsorbed solvent molecules in the adlayer. The dark troughs between the neighboring bright lamellas are packed with alkoxy chains, whose number is twice that of the alkoxy chains belonging to the DTCD molecules. The excess alkoxy chains are ascribed to the co-deposited 1-octanol molecules. They interact with the hydroxyl groups of DTCD molecules via solvent-solute hydrogen bonding. The DTCD molecules organized into another assembly structure when 1,2,4-tricholorbenzene (TCB) is used as solvent. A meshy structure with alternatively arranged dark holes and bright rods can be resolved clearly in Fig. 7d. In view of the shape and dimension, each bright rod is assigned as a DTCD molecule. Each dark hole is surrounded by four bright rods in a head-to-head configuration, as illustrated by the superimposed molecular model. The theoretical simulation indicates the existence of intermolecular hydrogen bonds between the hydroxyl groups of neighboring DTCD molecules, which is also responsible for the chirality of the adlayer.

3.4. Other experimental conditions

SAM of alkanethiol on gold surfaces is one of the most classical and intensively investigated systems because of its unique properties: ease of preparation and long-term stability. It is known that the formation of an alkanethiol SAM will undergo

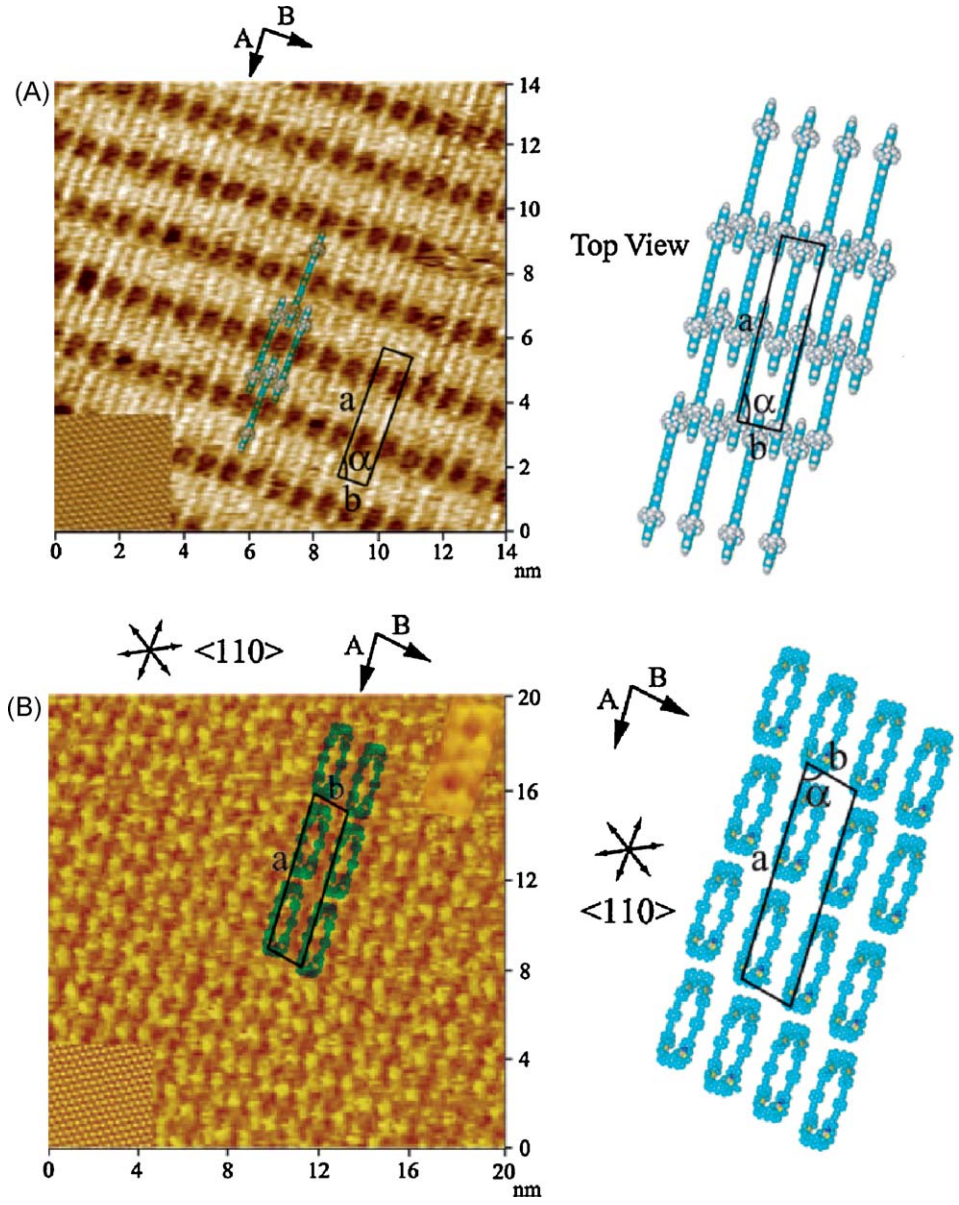

Fig. 6. STM images of highly ordered self-assembly of a supramolecular rectangle on HOPG (a) and on Au(111) surfaces (b) [69].

several stages from initial random adsorption to final densely packed ordered adlayer on a solid surface [48,78–80]. The time evolution of the self-assembly process has been monitored by STM [80]. The SAMs were prepared by immersing Au(1 1 1) into an ethanol solution containing 1 μM decanethiol with different immersion times. STM images shown in Fig. 8 reveal the formation process and adlayer structure of the SAMs. From 5 to 10 s (Fig. 8a), small domains with ordered molecular organization appears, although random molecules could be observed on Au(1 1 1) at the very initial stage. At 30 s (Fig. 8b), the SAM consists of uniform short stripes. Each stripe consists of sets of decanethiol molecules. Each set contains eight molecules arranged in a head-to-head configuration in most cases. With the elongation of the immersion time, the length of the stripes increases as well. At 5 min, the flat-lying alkyl chains become overcrowded on the surface and some overlapping between the adjacent stripes is observed (black circle in Fig. 8c). After immersing Au(1 1 1) in decanethiol solution for 3 days, a densely packed adlayer with a $(\sqrt{3} \times \sqrt{3})R30^\circ$ structure was observed, as shown in Fig. 8d. The formation process and structure of decanethiol SAMs are well related to the sample preparation conditions. The systematic study gives a clear picture about how the SAMs form and reveals the time-dependent dynamic process on the thiolate/Au interface. The SAM originates from random molecules at the very initial stage, and then shows nucleation with small molecular clusters, stable short stripes, stacking organization, and final dense structure. The molecules show a high mobility and actively reorganize on the Au(1 1 1) surface during the adlayer formation.

Zhang et al. reported the structural transition of a monodendron, 5-(benzyloxy)-isophthalic acid derivative ($C_{47}H_{76}O_7$, ab. BIC) molecule self-assembly tuned by the concentration-dependent solvent-solute interaction [81]. Fig. 9a is a typical large-scale STM image acquired in 1-octanol solution containing 5×10^{-4} M BIC molecules on HOPG surface. A lamellar structure with parallel bright stripes and dark troughs can be clearly seen. Each lamella consists of two molecular rows. Individual BIC molecules can be resolved in this image. The molecular pairs in a lamella take a head-to-head configuration and are interconnected by intermolecular hydrogen bond. The alkyl chains are packed interdigitally in between the bright stripes. With the decrease of solution

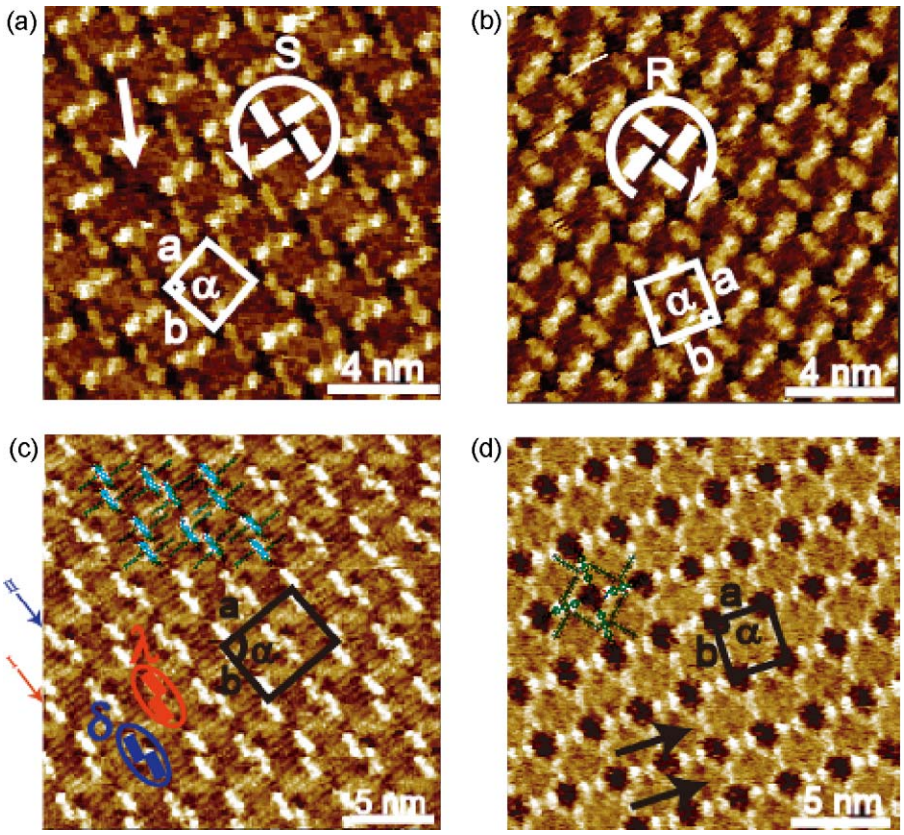

Fig. 7. (a and b) STM images of chiral domains of DTCD self-assembly on HOPG using THF as solvent. (c) STM image of racemic adlayer of DTCD on HOPG using octanol as solvent. (d) STM image of chiral adlayer of DTCD on HOPG using trichlorobenzene as solvent [76].

concentration, a quadrangular structure is observed, as shown in Fig. 9b. Four BIC molecules form a four-leaf-clover tetramer shape as the basic unit of the adlayer. In a tetramer, aromatic cores of four BIC molecules organize in a head-to-head configuration. Note that two pairs of short and less bright rods could be found between two neighboring tetramers. The short rods are attributed to 1-octanol molecules co-adsorbed in the assembly. They interact with BIC molecules through hydrogen bonding. When BIC sample was diluted to a concentration of less than 5×10^{-5} M, a hexagonal structure appears in BIC self-assembly. High-resolution STM image of Fig. 9c provides detailed information of the hexagonal structure. Three bright spots form a triangle as the basic unit of the self-assembly and occupy at the six corners of a hexagon. In the basic unit triangle, three aromatic cores from three BIC molecules form a trimer. The alkyl chains extend over HOPG surface and interdigitate each other to form the borders of the hexagons. The size of the vacancy in a hexagon is measured to be about 3.8 nm. Four shorter bright rods, in parallel to the four alkyl chains of two BIC molecules, are found in between the neighboring trimers. They are attributed to co-adsorbed 1-octanol molecules. The existence of strong adsorbate–solvent hydrogen bonding is concluded from the theoretical simulation. The sequential structural transition of BIC assembly from lamellar, quadrangular to hexagonal reflects the elaborate role of solvent-adsorbate interaction and solvent-substrate interaction in the solid/liquid interface assembly process. The similar concentration-dependent structure evolution has been observed in other systems [82,83].

3.5. Structural transition by external stimuli

3.5.1. Thermo treatment

The formation of surface self-assembly is a thermodynamic and kinetic process. It is well known that the thermo-annealing can induce the formation of ordered adlayer or new thermodynamic stable structure, and/or the enlargement of domain size [84]. For example, thermo-annealing can induce the structural transition of an alkyl substituted stilbenoid dendrimer from a hexagonal nanostructures at room temperature to a parallelogram nanostructure with a higher surface coverage at higher temperature [85].

Rohde et al study the trans–cis isomerization of a two-core dioxaborines (DOB) on HOPG surface induced by thermal annealing [86]. The DOB molecule adopts a coplanar trans-configuration at room temperature. A semiempirical simulation indicates that the trans–cis isomerization energy barrier of DOB is lower than that of azobenzene and stilbene. This lower energy barrier allows the DOB molecules to change their conformation by thermal stimulation. Fig. 10a shows a STM image of the 2D molecular assembly on HOPG. Two enantiomeric domains are clearly seen. Each domain consists of highly ordered molecular rows. The molecules form a lamellar structure with aligned bright spots, which can be attributed to the π-conjugated backbones of the molecules. The dodecyl chains are arranged in a comblike fashion between the neighboring bright π-conjugated backbones. The intermolecular hydrogen bonding is proposed as the driving force for the observed structures, as shown in the proposed structural model.

When the HOPG substrate is heated to 100 °C, the growth of domain size is observed. Further increasing the temperature to 130 °C results in the appearance of a new ordered structure. The high-resolution STM image of the new structure is shown in Fig. 10b. The new domain shows a hexagonal symmetry rather than the previously described lamellar structure. Each bright spot can be discerned as a trimer and surrounded by the interdigitated alkyl chains. Interestingly, this hexagonal domain is composed of the cis isomer of the molecules, as shown in the proposed structural model. The hydrogen bonding between the molecules is

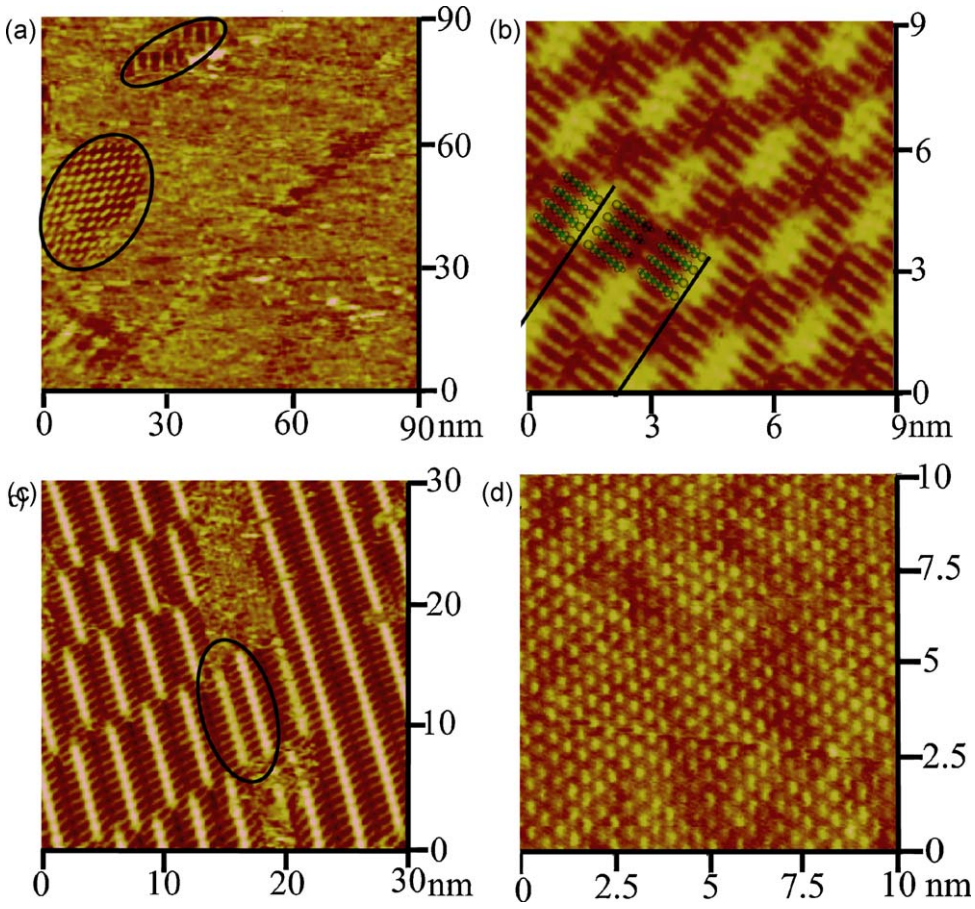

Fig. 8. STM images of adlayer of decanethiol on Au(1 1 1) prepared by dipping in thiol solution for 10 s (a), 30 s (b), 5 min (c), and 3 days (d) [80].

responsible for the formation of the trimers. The possible hydrogen bonding in the trimer is indicated by black dashed lines in the enlarged inset. The hydrogen bonding is considered to exist between the fluorine atoms of the BF_2 group and the hydrogen in the ortho position of the phenyl ring. The size of these hexagonal domains increases when the adlayer was heated to 150 °C. Finally, the hexagonal structure covers the entire substrate surface. As a sharp contrast, although the trans–cis transformation at 132 °C is identified by differential scan calorimetric (DSC) experiment, the cis isomers are unstable in solution. The formation of stable self-assembly from cis isomers on HOPG surface can be attributed to the van der Waals interaction of alkyl chains on HOPG.

3.5.2. Photo-irradiation

The surface photochemical reaction has been intensively investigated in the past years [7,87,88]. The widely studied reactions include photo-induced trans–cis isomerization of azobenzene [89–91], diarylethene [92], and photopolymerization of cinnamate [93,94], stilbene [95], and diacetylene [96,97]. The existence of intermolecular interaction and substrate–molecule interaction renders surface photochemical process some unique features. The latest progress on this topic has been reviewed recently [87].

Due to the large structural difference of photo-active molecules before and after photo-reaction, the surface photochemical reactions generally induce the noticeable structural transition in the adlayer. Xu and Wan studied the photo-isomerization of azobis-(benzo-15-crown-5) on Au(1 1 1) surfaces by STM [91]. Trans-azobis-(benzo-15-crown-5) molecules form a highly ordered array with molecular rows orientated along the close-packing direction of Au(1 1 1) substrate. Each molecule appears as a dumbbell shape with two dark depressions, which indicates it adopts a flat-lying configuration. In contrast, the adlayer of cis isomer on Au(1 1 1) consists of much smaller domains with

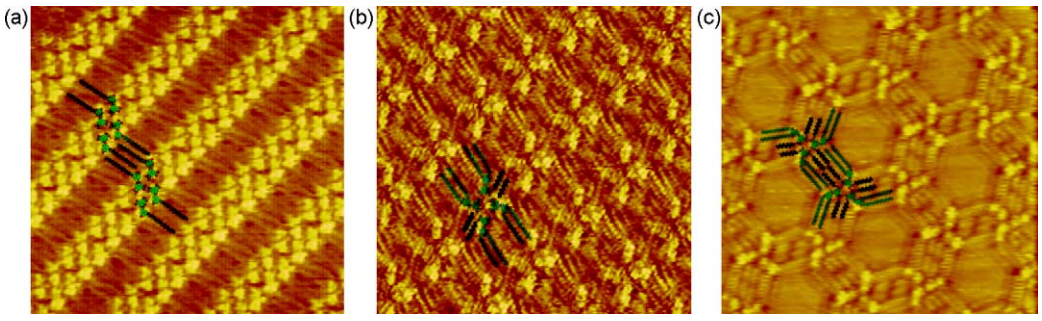

Fig. 9. STM images of BIC adlayer on HOPG at different concentrations [81].

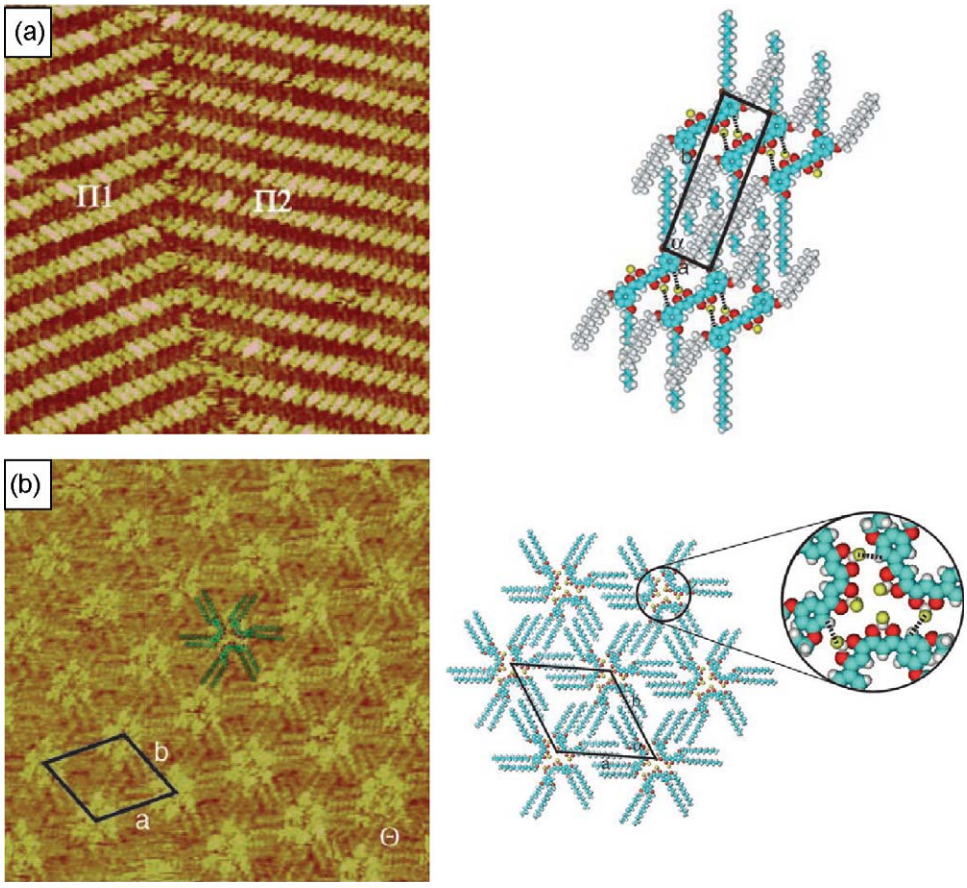

Fig. 10. (a) STM image and structural model of DOB adlayer on HOPG. (b) STM image and structural model of cis-DOB adlayer with hexagonal symmetry on HOPG obtained after heating the sample to 130 °C [86].

numerous defects. Each molecule appears as a "V" shape with two elongated spots, which can be assigned to the crown ethers of a cis-azobis-(benzo-15-crown-5) molecule. In situ irradiation on the stable adlayer of trans isomer results in the appearance of many bright clusters on the surface, along with the formation of disordered adlayer at the domain boundary. The strong spatial restriction imposed by neighboring molecules in the domain makes the trans isomers inside the ordered adlayer less prone to be isomerized.

In a few examples, however, the cooperative movement of photo-active groups results in the preservation of adlayer structure after photo stimuli. The representative example is the topochemical photopolymerization of diacetylene [96–98]. The diacetylene substituted with alkyl chains has been shown to self-organize into the well-ordered lamellar structures on HOPG. The diacetylene units appear as large bright spots stacking along the lamellar axis. Detailed analysis of the adlayer structure indicates that the stacking distance between two neighboring diacetylene units and the angle between the diacetylene rod and the stacking axis are well fit to the geometry requirement for the occurrence of topochemical polymerization in diacetylene crystal. The topochemical photopolymerization of diacetylene occurs after UV irradiation for 5 min. The brighter lines along lamella axis corresponding to the polymerized diacetylenes are observed in STM image. A great feature for topochemical reaction is that the adlayer almost preserves its structure before and after reaction. This reaction can also be induced by applying a negative bias pulse [99], which makes it possible to control the reaction at specific location.

Pace et al. demonstrated the collective switching of entire molecular 2D crystalline domains during the photo-isomerization of an azobenezene derivative SAM on a Au(1 1 1) surface [100]. The azobenzene moieties are orientated approximately perpendicular to the surface through Au–S bonds. When a UV light (365 nm) is introduced to activate the trans–cis isomerization, the collective movement of the azobenzene moieties in the SAM results in the formation of ordered cis conformer domains without disturbing the original unit cell established by the adsorption of trans conformers. The intermolecular interactions, presumably π–π interaction, are the driving force for the cooperative movement of the molecules and are responsible for the stability of the obtained cis conformer domains.

3.5.3. Potential control

The well-defined nanostructure can be constructed on solid surfaces or at solid/liquid interface under potential control with inorganic ions and organic molecules. Applying surface potential is an efficient way to modulate the surface self-assembly. In an electrochemical environment, there is a strong electric field in the double layer region [101]. The potential-dependent surface structural transition reflects the electric field modulated substrate–molecule interaction and/or intermolecular interaction change. The typical transition processes include order-disorder transition, adsorption orientation change, coverage transition, and others [102]. Many model compounds, such as pyridine [103], 2,2′-bipyridine [104,105], 4,4′-bipyridine [106,107], trimesic acid [108,109], have been shown to have potential-dependent adlayer transition process on electrode surfaces.

Beyond that, the electron transfer at the electrode/electrolyte interface can induce a series of interfacial chemical reaction, which provides a feasible way to construct surface nanostructures. Wen et al. reported the fabrication of oriented one-dimensional (1D)

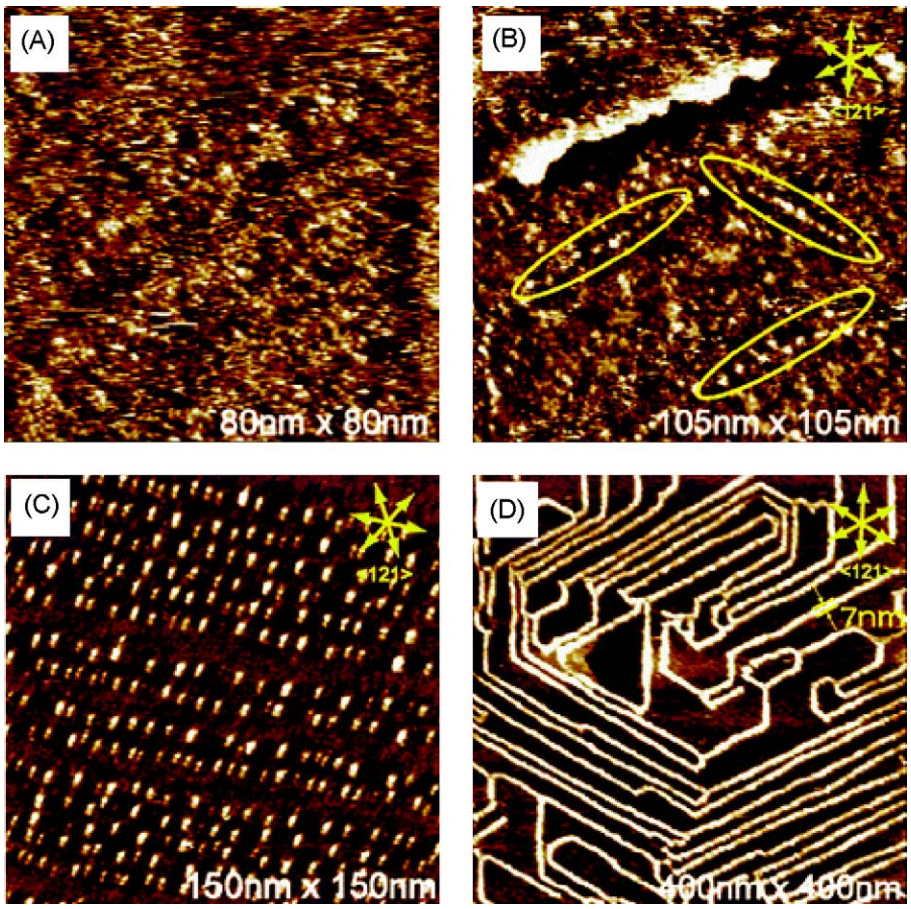

Fig. 11. Typical STM images of picric acid adlayer on Au(1 1 1) in 0.1 M $HClO_4$ at electrode potential of (a) 500 mV, (b) 360 mV, (c) 250 mV, and (d) 200 mV [110].

molecular chains on a Au(1 1 1) surface from nitrobenzene and picric acid [110]. The deposition process is monitored by in situ electrochemical scanning tunneling microscopy (ECSTM). Fig. 11 shows sequential STM images of Au(1 1 1) in a picric acid-containing solution. At 500 mV, a disordered adlayer is observed. When shifting the potential to 360 mV, some aligned bright clusters appear on the surface, as indicated by yellow ellipses in Fig. 11b. These clusters grow preferentially along ⟨1 1 2⟩ direction of Au substrate, which coincides with the orientation of Au(1 1 1) herringbone reconstruction. A well-defined chain pattern like a "circuit line" is seen at 200 mV, as shown in Fig. 11d. These oriented chains have a width of ca. 7 nm. Molecular aggregation and diffusion on a Au(1 1 1) surface in the reductive deposition is responsible for the formation of the oriented molecular islands and chains. In addition, the potential controlled fabrication of molecular 1D chain has been demonstrated by electropolymerization of thiophene and aniline derivatives [111,112].

3.5.4. Magnetic field

The modulation of surface chiral self-assembly by magnetic field has been demonstrated by a study of 4-cyano-4′-octylbiphenyl (8CB) on HOPG [113,114]. Although 8CB is an achiral liquid crystal molecule, the surface confinement effect quenches the chiral adsorption conformation of 8CB, and results in the formation of racemic adlayer. When applying a magnetic field (1.2 T) parallel to the substrate at the solid/liquid interface at 100 °C for 2 min, the alignment of 8CB molecules in solution phase is induced and "imprint" on the monolayer. As a result, a molecular film with a net excess of one enantiomorph over the other is observed by STM. Furthermore, the absolute chirality and enantiomeric excess in 8CB monolayers can be controlled by adjusting magnetic field orientation with respect to the ⟨1 1 0 0⟩ direction of graphite substrate.

4. Multicomponent self-assembly

Multicomponent self-assembly is an ultimate approach to build up desirable nanostructures with specific functionality. Ideally, the structures and the functionality are determined by different components, although phase separation is frequently observed in often time. The insight understanding of surface assembly and structural transition process of monocomponent supramolecular structure provides valuable knowledge to explore the multi-component assembly. Through careful molecule design, the sophisticated surface architectures can be obtained by co-adsorption, host–guest interactions, multilayer assembly and others.

4.1. Co-adsorption

It is well known that alkane and its derivatives can form highly ordered lamella structures on HOPG surface. These lamella structures have been used to guide the assembly of molecular chain of phthalocyanine derivates. Fig. 12 shows a typical STM of co-adsorbed copper(II)-octabutoxy-phthalocyanine (CuPcBu8) and 1-iodooctadecane (C18I) [115]. As expected, 1-iodooctadecane forms long-ranged ordered lamella structure, which templates the assembly of CuPCBu8 into one-dimensional molecular chains. The molar ratio of CuPcBu8 to C18I is estimated to be 1:4 from the STM images. The carbon skeleton of 1-iodooctadecane orientated at an

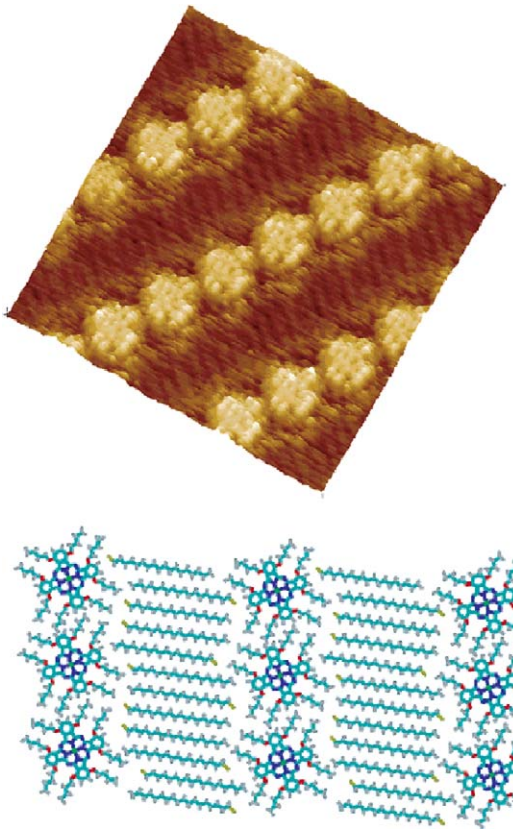

Fig. 12. High-resolution STM image (12 nm × 12 nm) and molecular model for the assembly structure of 1-iodooctadecane with CuPcBu8 [115].

angle of 81 ± 4° with respect to the CuPcBu8 molecular array. The interaction between the Pc and C18I molecules is considered mainly van der Waals force. Similarly, the construction of one-dimensional assembly of unsubstituted phthalocyanine has also been achieved when co-adsorbed with alkane halides and thiols [116].

The interface assembly of porphyrin or phthalocyanine on solid substrates has attracted a great deal of attention due to the fundamental and technological interests in the fields of biology, photosynthesis, electrocatalysis, and molecular devices [117]. The formation of ordered binary co-assembly of CoPc (cobolt phthalocyanine) and CuTPP (copper tetraphenylporphyrin) on Au(1 1 1) and Au(1 0 0) surfaces has been reported [118,119]. The adlayer was prepared by immersing gold surfaces into a benzene solution containing both CoPc and CuTPP and characterized by ECSTM. At proper experiment condition, an ordered 2D binary array of CoPc and CuTPP is obtained on Au(1 0 0)-(hex) and Au(1 1 1). As shown in Fig. 13, alternately arranged molecular rows are uniformly formed on Au(1 0 0)-(hex). Molecular row I is composed of CoPc, which can be recognized as a propeller-shaped feature with a central brightest spot and four symmetric spots at the corners. On the other hand, the individual molecule in row II shows a ring shape with a dark spot in the center, indicating that it is a CuTPP molecule. In contrast, when Au(1 0 0)-(1 × 1) was used as the substrate, a disordered structure was found, suggesting that the reconstructed Au(1 0 0)-(hex) surface is a key factor in controlling alternate CoPc and CuTPP molecular chains.

Nanopatterned hybrid adlayer architectures composed of 1,4-bis(4-pyridylethynyl)-2,3-bis-dodecyloxy-benzene (PBP) and an oligo-thiophene derivative DTT have been successfully fabricated on an HOPG surface [120]. The co-adsorption of two-component mixtures of PBP and DTT results in a variety of hybrid nanopatterned architectures that differ from their respective mono-component surface assemblies. The hybrid structures are

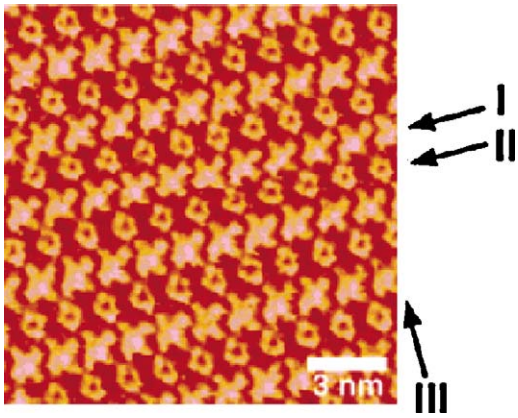

Fig. 13. High-resolution STM image (15 nm × 15 nm) of CoPc and CuTPP mixed adlayer formed on Au(1 0 0)-(hex) surface in 0.1 M $HClO_4$ [118].

highly dependent on the molar ratio of PBP to DTT. The increase in the molar ratio of PBP to DTT results in a parallel, although less dramatic, increase in the ratio of PBP to DTT in the unit cell of each ordered adlayer. Intermolecular adsorbate–adsorbate interactions play a dominant role in the formation of hybrid adlayer structures. STS measurements indicate that the molecular energy levels of PBP and DTT on an HOPG surface are relatively insensitive to changes in the hybrid supramolecular architectures.

Gong et al. reported a result on the fabrication of ordered molecular aggregates through co-adsorption [121]. An oligo(phenylene-ethynylene) (OPE) molecule with carboxylic acid end group and flexible side alkyl chains is chosen as a template molecule. Fig. 14a shows the chemical structures of OPE and coronene (COR) guest molecule. At a 1:2 molar ratio of COR to OPE, co-adsorption of the two molecules results in a homogeneous molecular self-assembly. Fig. 14b is a high-resolution STM image showing the molecular network with bright lines and dark parallelograms. The bright straight lines are ascribed to the OPE conjugated backbones. The alkoxyl chains of OPE oligomer are interdigitated in between the OPE lines. A distinguishing feature in the image is the round bright spots distributed in between the alkoxyl chains. The diameter of the round spots is measured to be ca. 0.95 nm, consistent with the molecular diameter of COR. Therefore, the bright round spots are assigned to COR molecules dispersed in the alkoxyl chains of the OPE template. The coverage of COR is 0.089 molecule/nm^2. When the molar ratio of COR/OPE is adjusted to 1:1, a new self-assembly of COR in OPE template is observed as shown in Fig. 14c. It is clear that two COR molecules exist in every space of OPE template. With the accommodation of a COR dimer, the space provided by the molecular template is almost fully occupied. As a result, COR molecules are well stabilized and well resolved by STM. The surface coverage of COR molecules is increased to 0.177 molecule/nm^2. Controllable distribution of COR can be continually achieved. Fig. 14d is a typical STM image acquired on the molecular network when the concentration ratio of COR to OPE is 3:2. Two types of COR molecular arrays can be seen in the image marked by arrows I and II. In array I, a single COR molecule is filled within the space of OPE template, while a pair of molecules is in array II. A COR coverage of 0.214 molecule/nm^2 is yielded in this structure. In a similar way, the uniform distribution of tripeptide and CdSe nanoparticles can be achieved using OPE template.

More sophisticated nanostructure can be achieved by multi-component co-adsorption. Recently, three and four-component two-dimensional highly ordered nanostructures have been reported [122,123]. Fig. 15 shows a high-resolution STM image of assembly formed by a fused dehydrobenzo[12]annulene

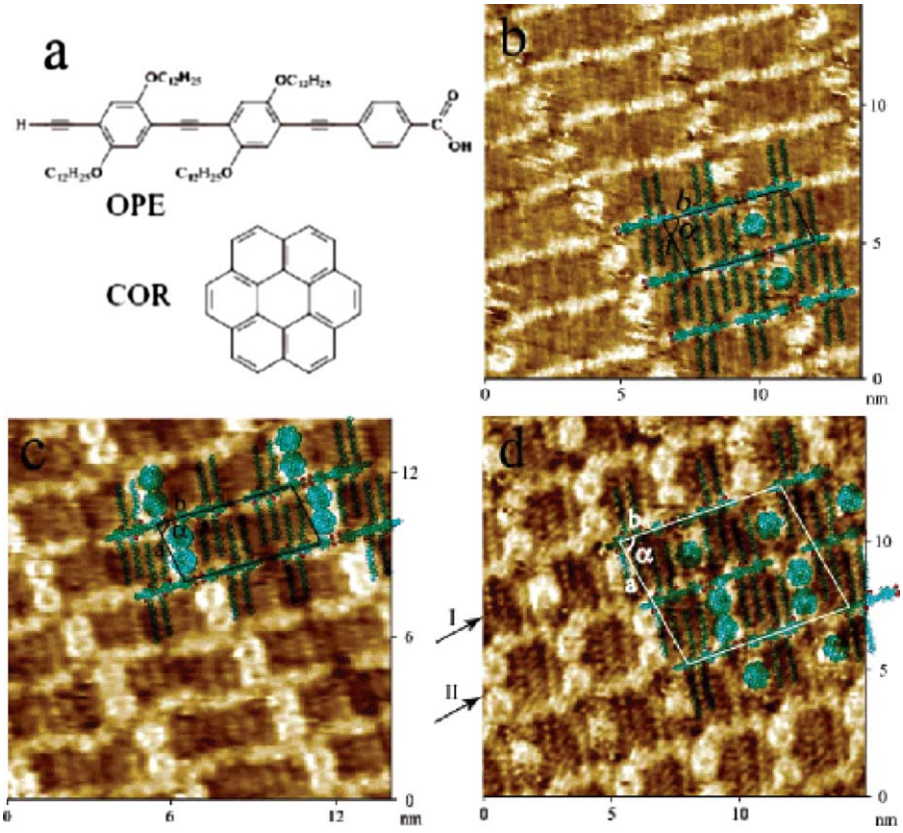

Fig. 14. (a) Chemical structures of OPE and COR, (b) high-resolution STM image of one by one distribution of COR, (c) high-resolution STM image of two by two distribution of COR, and (d) high-resolution STM image of one by two distribution of COR [121].

derivative (bisDBA-C_{12}), corenene, isophthalic acid, and triphenylene [123]. A Kagome structure is formed by bisDBA-C_{12} and covers the entire surface. Each hexagonal void is filled with a $corene_1$-$isophthalic\ acid_6$ cluster. The triangular voids are filled by triphenylene molecules. The structure model is presented in Fig. 15b. Not surprisingly, the formation of this beautiful nanostructure requires delicately adjusting the experimental conditions, such as concentration, molar ratio between each component, and solvent. Nevertheless, the result demonstrates the possibilities to obtain complicated nanostructures through self-assembly technique.

4.2. Host–guest assembly

As a representative concept in supramolecular chemistry, host–guest chemistry has been borrowed to build up 2D supramolecular assembly nanostructures. For example, the ordered 2D array of C60 can be obtained through the host–guest self-assembly technique. Calixarene are well studied as host molecules for a variety of guest molecules, including C60. It has been demonstrated that calixarene can self-assemble into ordered array on Au(1 1 1) surface [124–126]. In contrast, due to its high mobility on surface, C60 itself cannot self-assemble into long-range ordered adlayer on Au(1 1 1) at room temperature [127]. Taking advantage of the host–guest interaction of calixarene and C60, a highly ordered array of C60 was constructed using the calix[8]arene array as a template [128]. The formation of ordered adlayer can be attributed to the self-assembly behavior of calixarene.

A prerequisite for the surface host–guest assembly is to build up versatile open porous network structures as template. The formation of nanoporous self-assembly on surfaces has been observed in many systems [129]. The driving force for the supramolecular networks can be metal-organic coordination interaction [130–132], hydrogen bonds [75,133–135], or van der Waals interactions[136–138]. The common character of these templates is the existence of highly ordered cavities. The existence of ordered array of cavities invites the inclusion of guest molecules or other nano-objects to fabricate ordered pattern of functional molecules or nano-materials. This surface host–guest self-assembly process is a close analogue to the solution phase host–guest chemistry and has attracted great attention due to the potential applications in molecular electronics, ultrahigh density data storage, nanopatterning, and others. The unique feature of this approach is that the arrangement of the guest molecules on the surface is predefined and can be tuned by the host template.

The nanoporous network of a triple-armed amphiphile, 1,3,5-tris(10-carboxydecyloxy)benzene (TCDB), has been extensively used as a template for the fabrication of ordered array of functional molecules. TCDB is a derivative of trimesic acid and can form two-dimensional networks on HOPG with well-defined nanoscale cavities [139]. Fig. 16a is a representative STM image of the TCDB adlayer acquired on HOPG. Each TCDB molecule can be recognized as one bright spot, the benzene core, and three chains, the carboxydecyloxy "arms," consistent with its chemical structure. An important structural feature in the image is the existence of quasi-rectangular cavities, indicated by ovals, framed by intermolecular hydrogen bonds connected alkyl chains from neighboring molecules. As measured with STM, the size of the cavity is about 2.4 nm × 1.3 nm. The highly ordered nanoporous network structure provides an excellent host template to regulate the distribution of guest molecules on surfaces. A number of functional organic molecules such as coronene, phthalocyanine, and decacyclene, have been used as guest molecules to demonstrate the versatility of the TCDB template [139,140]. Shown in Fig. 16b is a STM image of an ordered array of a supramolecular rectangle in TCDB host template [141]. The dark vacancies in the TCDB adlayer have been

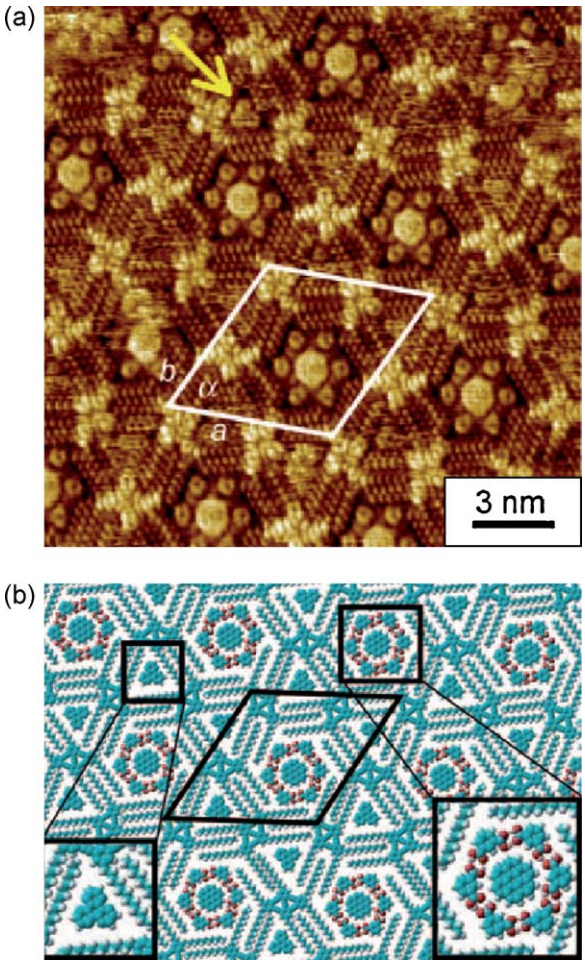

Fig. 15. (a) STM image and (b) proposed structural model of a mixture of bisDBA-C12, coronene, isophthalic acid, and triphenylene [123].

filled with a bright, elongated feature, which can be ascribed to the entrapped supramolecular rectangle. The dimension of the bright oval is measured to be 2.1 nm × 1.2 nm, consistent with the size of the supramolecular rectangles. In contrast, a disordered adsorption of supramolecular rectangles is observed without TCDB. Detailed structural analysis indicates that the TCDB template slightly adjusts its dimension to accommodate the entrapped rectangles.

The effect of thermo-annealing to the host–guest assembly was carried out. At room temperature, VOPc (vanadyl phthalocyanine) can be hosted by TCDB template to form a dimer-entrapped architectures [142]. Upon thermal-annealing at 90 °C, a structural transition from a dimer-entrapped architecture to a monomer-entrapped one is observed. Fig. 16c and d displays the typical high-resolution STM images of two types of the binary complex architectures. The conjugated VOPc molecules appear as bright spots can be clearly identified in the STM images, as highlighted by white squares. The TCDB molecules surrounding the VOPc guest molecules can also be resolved. The positions of benzene cores of TCDB are drawn with white circles to guide the eyes. The detailed structural analysis indicates that the host cavities of TCDB expand or reduce in response to the guest architectures. Such host structure flexibility is achieved by the alkyl chain distortion and the hydrogen bond switching of host networks. DFT calculations show that the interaction of hydrogen bonding in the monomer entrapped architecture is much stronger than that in the dimer entrapped one. The observed phase transition from dimer-entrapped structure to monomer-entrapped structure is proposed to be associated with the competition between the thermal motions of the molecules and the stability of hydrogen bonding in TCDB dimers.

Li and coworkers use Kagomé open networks formed by a tetraacidic azobenzene molecule NN4A to direct the assembly fullerenes on surface. Two types of cavities with different size and symmetry exist in a NN4A adlayer. The larger A-type cavity with six-fold symmetry is framed by six benzene rings connected through hydrogen bonds between the carboxylic groups. The cavity diameter is about 12.0 Å. On the other hand, the smaller B-type cavity is formed from three NN4A molecules arranged in a triangular shape. The inner width is measured to be about 8.6 Å. These cavities are capable of accommodating fullerene molecules as guest species. Interestingly, the host–guest assembly process shows appreciable size selectivity. For example, both the A- and B-type cavities are large enough in diameter to accommodate guest molecules such as C60. The larger C80 and Sc3N@C80 molecules, however, are trapped exclusively in the A-type cavities. The theoretical simulation results match well with the experiment observation.

4.3. Self-assembly in vertical direction

Parallel to the development of 2D supramolecular assembly, it is also of great interest to build up advanced structures in vertical direction. The epitaxial growth of homogeneous or, more interestingly, heterogeneous film is important to build up molecular junction, charge and energy transfer complex, organic electronic devices, etc.

In fact, the formation of multilayer assembly has been observed in many systems, both at submonolayer coverage, or multilayer coverage. The observations of the bilayer structures of phthalocyanine and tetrathiafulvalene (TTF) derivatives on graphite surfaces have been reported previously. The high-resolution STM images of octa-alkoxyl-substituted phthalocyanine (PcOC8) adlayer indicate a 0.40 nm shift of the overlayer assembly along one of the unit cell direction [143]. The bilayer structures are simulated by molecular mechanics method and the calculated results agree well with the experimental observation, indicating that the observed overlayer shift could be attributed to the π–π interaction between phthalocyanine cores in the upper layer and lower layer. Similarly, an alkyl substituted TTF derivatives also show the formation of π–π interaction induced double layer structure at high concentration [144,145]. The shift of the TTF cores of the upper layer is very little relative to the bottom layer, as confirmed from both experiment observation and theoretical modeling.

The decker sandwich complexes of porphyrin have unique three-dimensional structure and are promising candidates for being used in molecular machine, organic field-effect transistors, liquid crystals, and chemical sensors. Otsuki et al. reported the assembly of the double-decker porphyrin complexes of cerium(IV) [146]. The shape of the upper ring is reflected in the STM image with circular, square, and elliptic features, depending on the structure of upper porphyrin derivatives. When co-assembled with un-complexed porphyrin molecules, the double-decker complexes are distinguishable with brighter features. Yoshimoto et al investigated the assembly of a triple-decker porphyrin/phthalocyanine/phthalocyanine Eu complex on an Au(1 1 1) surface [147]. By sweeping the electrode potential from 0.77 to 0.02 V, a reversible structural change from square unit cell adlayer to a hexagonal arrangement is observed, which is related to the surface charge change controlled by the electrode potential.

The more interesting way to build up three-dimensional nanostructures is taking advantage of the supramolecular intermolecular interactions. Yoshimoto et al. demonstrated the construction of C60 array using zinc(II) octaethylporphyrin

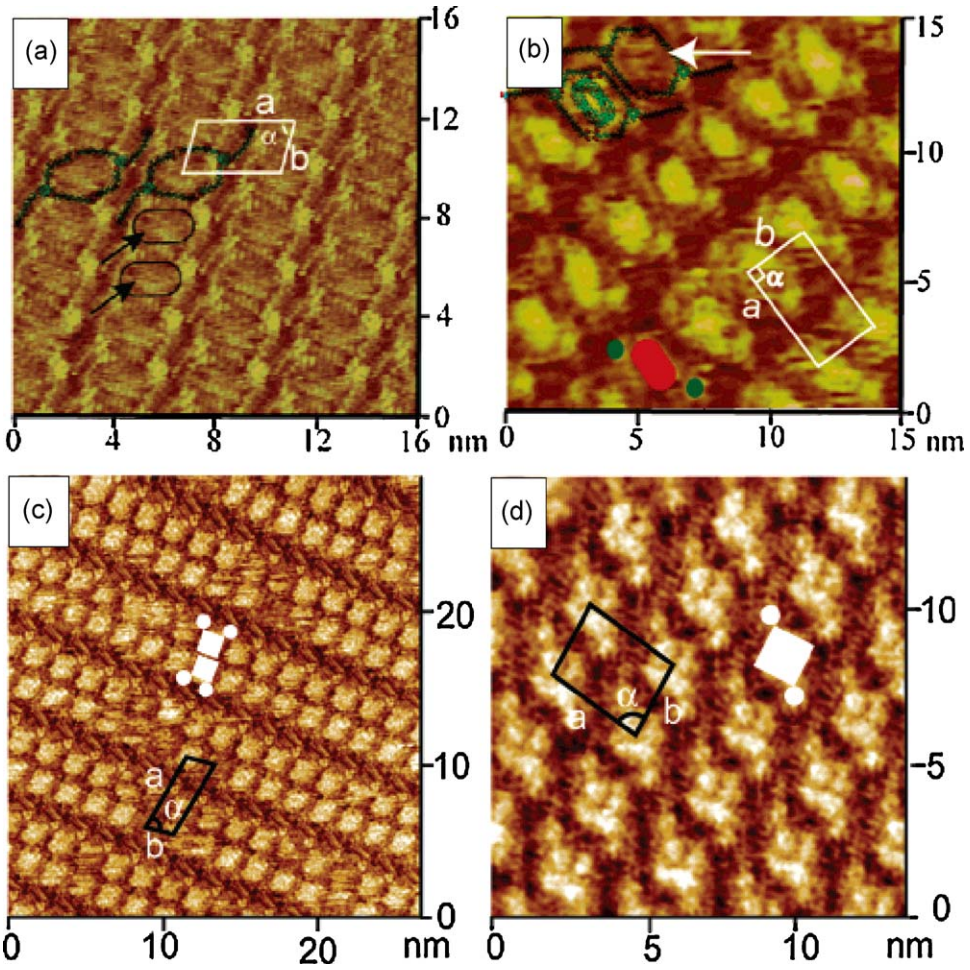

Fig. 16. (a) STM image of TCDB adlayer on HOPG showing the existence of ordered cavities, (b) STM image of host–guest assembly of supramolecular rectangles in TCDB molecular template [141], (c) dimer-trapped and (d) monomer-trapped adlayer of VOPc in TCDB template [142].

[Zn(OEP)] as docking molecule on Au(1 1 1) surface [148]. The self-assembly process was completed by sequentially dipping an Au(1 1 1) surface into a benzene solution of Zn(OEP) and that of an open cage C60 derivative. A highly ordered array of the C60 cage on the Zn(OEP) modified Au(1 1 1) adlayer was seen in the STM image (Fig. 17). Each complex appears as a bright spot in the STM images. In contrast, a disordered structure was found when the C60 cage molecules were directly attached to the Au(1 1 1) surface. Because of the specific interaction of Zn(OEP) and C60 cage, all of the C60 cage molecules have the same orientation in the adlayer, which is confirmed by electrochemical measurement. A similar ordered assembly of the C60 cage is also observed on the Zn(OEP) modified Au(1 0 0)-hex surface [149]. Interestingly, aggregates of opened C60 formed on the ordered Zn(OEP)-modified Au(1 0 0)-(1 × 1) surface. As a result, poor electrochemical response of the C60 cage is found on Zn(OEP)-modified Au(1 0 0)-(1 × 1). The difference in surface charge of the unreconstructed Au(1 0 0)-(1 × 1) and the reconstructed Au(1 0 0)-(hex) surface is thought to affect the molecular recognition between the opened C60 cage and Zn(OEP). Similarly, the ordered adlayer of a C60 derivative with ferrocene

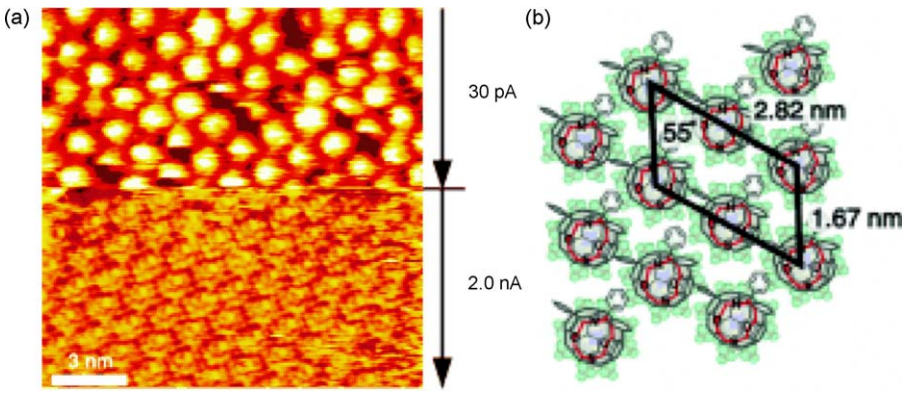

Fig. 17. (a) Composite STM image of C60 cage/Zn(OEP) adlayer showing the upper layer (upper panel) and bottom layer (lower panel) and (b) proposed structural model [148].

group (C60Fc) was obtained on a porphyrin modified Au(1 1 1) substrate [150]. In situ STM observation revealed that C60Fc formed highly ordered arrays on the ZnOEP-modified Au(1 1 1) surface in the reduced form, whereas surface morphology showed a structural change at the potentials of the oxidized form. In addition, C60Fc molecule is not able to assemble on the FeClOEP-modified Au(1 1 1) surface due to the steric hindrance brought out by the axis coordinated Cl on the Fe ion.

Lei et al. demonstrated the formation of benzoic acid lines on tridodecylamine (TDA) modified HOPG surface [151]. TDA molecules self-assemble into well-ordered lamella structure with amino group at the center of the lamella. Applying a benzoic acid solution to the TDA adlayer results in the formation of the molecular lines along the center of the lamella. The hydrogen bonding between carboxylic acid group and amino group is responsible for the site-selective assembly. In a similar strategy, the decoration of an fatty acid derivative and a bipyridine derivative with urea or palladium(II) acetate on surface has been demonstrated [152,153].

5. Conclusions and outlook

Self-assembly is a ubiquitous and important process in nature. Adsorption and self-assembly at surface and interface is a key physical chemistry subject due to its close relationship to many fundamental and application scientific questions like catalysis, chirality, electron and energy transfer, single molecule science, and organic electronics. With the development of nanoscience and nanotechnology, self-assembly is increasingly being recognized as a representative approach in "bottom-up" technique for the fabrication of molecular nanostructure. The invention of STM and development of other surface characterization techniques give us the ability to study the self-assembly process with unprecedented preciseness.

Understanding the basic physical chemistry mechanism of adsorption and self-assembly on surface and interface is a fundamental step towards building it in a controllable way. As is well known, the surface self-assembly is driven by the interplay between molecule–substrate interaction and intermolecular interaction. The molecule–substrate interaction can guide the orientation of the molecules in the adlayer, whereas the intermolecular interactions are responsible for the formation of ordered molecular nanostructures in two-dimension. The detailed understanding of the driving force for the self-assembly process makes it possible to tailor the self-assembly process. This can be achieved in a straightforward way, such as changing the substrate and modifying the chemical structure of molecule, or more delicately, changing the environment, such as solvent, concentration, temperature, electric field, photo-irradiation, and others. At the same time, the construction of more complicated multiple components assembly has been explored through co-adsorption and host–guest assembly. The sophisticated nanostructures with multiple components have deepened the insight of self-assembly and enriched the content of supramolecular chemistry.

The results mentioned here only provide a cursory browse of some progress on constructing surface molecular nanostructures via self-assembly. Due to the inherent complexity of the surface self-assembly process, our understanding of the self-assembly is far from completed. In often time, the excitement brought from the intriguing experiment observation is offset by the frustration on the course to understand the underlying physical chemistry. The input from other fields, such as theoretical modeling and surface spectroscopic techniques, is highly demanded to help us get quantitative information of the self-assembly.

The advanced architectures built from functional molecules give us new platforms to detect molecular properties with atomic precision. Some interesting attempt has been made to study the adsorption, diffusion, desorption of single molecule in a confined space, such as surface nanoporous structure [154]. The single molecular chemical reaction study is highly expected. The single molecule physical and chemical property study will benefit a wide range of fundamental or application fields, such as catalysis, chirality origin, and molecular electronics.

In the context of nanotechnology applications, the promising perspectives for surface 2D ordered structures are nanopatterning and high density data storage. Low cost, fast, and high-resolution are all great features for self-assembly technique to be used in nanolithography. One of the biggest issues in this direction need to be demonstrated is the compatibility with the existing lithography techniques. In addition, very little attention has been paid to control the assembly of functional nano-objects, such as nanoparticles through surface molecular engineering approach. We believe the self-assembly technique has a bright future in nanofabrication applications.

With the rapid development in the past 20 years, we have accumulated valuable information about the surface self-assembly. A wealth of insight into the fundamental physical chemistry of self-assembly allows us to tune the 2D nanostructures by changing the chemical structure or adjusting the physical chemistry environment. It can be predicted that as the growth of understandings of the rules in the nanoscale, our dream to manipulate atoms and molecules could be realized in future.

Acknowledgements

The authors thank the financial supports form National Natural Science Foundation of China (Grants 20733004, 20821003, 20821120291, and 20905069), National Key Project on Basic Research (Grant 2006CB806100 and 2006CB932104), and the Chinese Academy of Sciences.

References

[1] J.V. Barth, G. Costantini, K. Kern, Nature 437 (2005) 671–679.
[2] L.J. Wan, Acc. Chem. Res. 39 (2006) 334–342.
[3] G. Binnig, H. Rohrer, Helv. Phys. Acta 55 (1982) 726–735.
[4] D.P.E. Smith, H. Horber, C. Gerber, G. Binnig, Science 245 (1989) 43–45.
[5] S. De Feyter, F.C. De Schryver, J. Phys. Chem. B 109 (2005) 4290–4302.
[6] S. De Feyter, F.C. De Schryver, Chem. Soc. Rev. 32 (2003) 139–150.
[7] S. De Feyter, A. Gesquiere, M.M. Abdel-Mottaleb, P.C.M. Grim, F.C. De Schryver, C. Meiners, M. Sieffert, S. Valiyaveettil, K. Mullen, Acc. Chem. Res. 33 (2000) 520–531.
[8] L.C. Giancarlo, G.W. Flynn, Acc. Chem. Res. 33 (2000) 491–501.
[9] J.V. Barth, Annu. Rev. Phys. Chem. 58 (2007) 375–407.
[10] S.M. Barlow, R. Raval, Surf. Sci. Rep. 50 (2003) 201–341.
[11] Q. Chen, H.J. Yan, C.J. Yan, G.B. Pan, L.J. Wan, G.Y. Wen, D.Q. Zhang, Surf. Sci. 602 (2008) 1256–1266.
[12] J.P. Rabe, S. Buchholz, Science 253 (1991) 424–427.
[13] S. Cincotti, J.P. Rabe, Appl. Phys. Lett. 62 (1993) 3531–3533.
[14] Z.X. Xie, X. Xu, J. Tang, B.W. Mao, Chem. Phys. Lett. 323 (2000) 209–216.
[15] L.E. Firment, G.A. Somorjai, J. Chem. Phys. 66 (1977) 2901–2913.
[16] L.E. Firment, G.A. Somorjai, J. Chem. Phys. 69 (1978) 3940–3952.
[17] G. Watel, F. Thibaudau, J. Cousty, Surf. Sci. Lett. 281 (1993) 297–302.
[18] Z.-X. Xie, X. Xu, B.-W. Mao, K. Tanaka, Langmuir 18 (2002) 3113–3116.
[19] R. Hentschke, L. Askadskaya, J.P. Rabe, J. Chem. Phys. 97 (1992) 6901–6909.
[20] S.-X. Yin, C. Wang, X.-H. Qiu, B. Xu, C.-L. Bai, Surf. Interface Anal. 32 (2001) 248–252.
[21] A.J. Groszek, Adsorption at the Gas–Solid and Liquid–Solid Interface, Elsevier, New York, 1982.
[22] A.J. Groszek, Proc. R. Soc. Lond. Ser. A 314 (1970) 473–498.
[23] H.M. Zhang, Z.X. Xie, B.W. Mao, X. Xu, Chem. Eur. J. 10 (2004) 1415–1422.
[24] K. Uosaki, R. Yamada, J. Am. Chem. Soc. 121 (1999) 4090–4091.
[25] R. Yamada, K. Uosaki, J. Phys. Chem. B 104 (2000) 6021–6027.
[26] A. Marchenko, J. Cousty, L.P. Van, Langmuir 18 (2002) 1171–1175.
[27] O. Marchenko, J. Cousty, Phys. Rev. Lett. 84 (2000) 5363–5366.
[28] Z.X. Xie, X. Xu, J. Tang, B.W. Mao, J. Phys. Chem. B 104 (2000) 11719–11722.
[29] L.C. Giancarlo, G.W. Flynn, Annu. Rev. Phys. Chem. 49 (1998) 297.
[30] D.M. Cyr, B. Venkataraman, G.W. Flynn, Chem. Mater. 8 (1996) 1600–1615.
[31] H.M. Zhang, J.W. Yan, Z.X. Xie, B.W. Mao, X. Xu, Chem. Eur. J. 12 (2006) 4006–4013.
[32] F. Tao, Y.G. Cai, S.L. Bernasek, Langmuir 21 (2005) 1269–1276.

[33] L.C. Giancarlo, H.B. Fang, S.M. Rubin, A.A. Bront, G.W. Flynn, J. Phys. Chem. B 102 (1998) 10255–10263.
[34] L. Giancarlo, D. Cyr, K. Muyskens, G.W. Flynn, Langmuir 14 (1998) 1465–1471.
[35] S. Buchholz, J.P. Rabe, Angew. Chem. Int. Edit. 31 (1992) 189–191.
[36] S.X. Yin, C. Wang, Q.M. Xu, S.B. Lei, L.J. Wan, C.L. Bai, Chem. Phys. Lett. 348 (2001) 321–328.
[37] M. Hibino, A. Sumi, H. Tsuchiya, I. Hatta, J. Phys. Chem. B 102 (1998) 4544–4547.
[38] F. Tao, J. Goswami, S.L. Bernasek, J. Phys. Chem. B 110 (2006) 4199–4206.
[39] F. Tao, J. Goswami, S.L. Bernasek, J. Phys. Chem. B 110 (2006) 19562–19569.
[40] S.L. Xu, S.X. Yin, H.P. Liang, C. Wang, L.J. Wan, C.L. Bai, J. Phys. Chem. B 108 (2004) 620–624.
[41] D.M. Cyr, B. Venkataraman, G.W. Flynn, A. Black, G.M. Whitesides, J. Phys. Chem. 100 (1996) 13747–13759.
[42] S.-X. Yin, C. Wang, Q.-M. Xu, S.-B. Lei, L.-J. Wan, C.-L. Bai, Chem. Phys. Lett. 348 (2001) 321–328.
[43] Q.M. Xu, L.J. Wan, C. Wang, C.L. Bai, Surf. Interface Anal. 32 (2001) 256–261.
[44] F. Tao, S.L. Bernasek, Chem. Rev. 107 (2007) 1408–1453.
[45] P.E. Laibinis, G.M. Whitesides, D.L. Allara, Y.T. Tao, A.N. Parikh, R.G. Nuzzo, J. Am. Chem. Soc. 113 (1991) 7152–7167.
[46] C.D. Bain, E.B. Troughton, Y.T. Tao, J. Evall, G.M. Whitesides, R.G. Nuzzo, J. Am. Chem. Soc. 111 (1989) 321–335.
[47] Z.Y. Li, S.C. Chang, R.S. Williams, Langmuir 19 (2003) 6744–6749.
[48] G.E. Poirier, Chem. Rev. 97 (1997) 1117–1127.
[49] L.H. Dubois, R.G. Nuzzo, Annu. Rev. Phys. Chem. 43 (1992) 437–463.
[50] M.C. Daniel, D. Astruc, Chem. Rev. 104 (2004) 293–346.
[51] G.M. Whitesides, E. Ostuni, S. Takayama, X.Y. Jiang, D.E. Ingber, Annu. Rev. Biomed. Eng. 3 (2001) 335–373.
[52] J.C. Love, L.A. Estroff, J.K. Kriebel, R.G. Nuzzo, G.M. Whitesides, Chem. Rev. 105 (2005) 1103–1169.
[53] E. Menard, M.A. Meitl, Y.G. Sun, J.U. Park, D.J.L. Shir, Y.S. Nam, S. Jeon, J.A. Rogers, Chem. Rev. 107 (2007) 1117–1160.
[54] A. Stabel, R. Heinz, J.P. Rabe, G. Wegner, F.C. Deschryver, D. Corens, W. Dehaen, C. Siiling, J. Phys. Chem. 99 (1995) 8690–8697.
[55] A. Stabel, P. Herwig, K. Mullen, J.P. Rabe, Angew. Chem. Int. Edit. 34 (1995) 1609–1611.
[56] A. Stabel, J.P. Rabe, Synth. Met. 67 (1994) 47–53.
[57] S. Ito, M. Wehmeier, J.D. Brand, C. Kubel, R. Epsch, J.P. Rabe, K. Mullen, Chem. Eur. J. 6 (2000) 4327–4342.
[58] V.S. Iyer, K. Yoshimura, V. Enkelmann, R. Epsch, J.P. Rabe, K. Mullen, Angew. Chem. Int. Ed. 37 (1998) 2696–2699.
[59] X.H. Qiu, C. Wang, Q.D. Zeng, B. Xu, S.X. Yin, H.N. Wang, S.D. Xu, C.L. Bai, J. Am. Chem. Soc. 122 (2000) 5550–5556.
[60] X.H. Qiu, C. Wang, S.X. Yin, Q.D. Zeng, B. Xu, C.L. Bai, J. Phys. Chem. B 104 (2000) 3570–3574.
[61] H.N. Wang, C. Wang, Q.D. Zeng, S.D. Xu, S.X. Yin, B. Xu, C.L. Bai, Surf. Interface Anal. 32 (2001) 266–270.
[62] L. Askadskaya, C. Boeffel, J.P. Rabe, Ber. Bunsen Phys. Chem. 97 (1993) 517–521.
[63] F. Charra, J. Cousty, Phys. Rev. Lett. 80 (1998) 1682–1685.
[64] P. Wu, Q.D. Zeng, S.D. Xu, C. Wang, S.X. Yin, C.L. Bai, ChemPhysChem 2 (2001) 750.
[65] Q. Chen, T. Chen, G.B. Pan, H.J. Yan, W. Song, L.J. Wan, Z.T. Li, Z.H. Wang, B. Shang, L.F. Yuan, J.L. Yang, Proc. Natl. Acad. Sci. U.S.A. 105 (2008) 16849–16854.
[66] S.L. Yau, Y.G. Kim, K. Itaya, J. Am. Chem. Soc. 118 (1996) 7795–7803.
[67] S. Yoshimoto, Y. Honda, O. Ito, K. Itaya, J. Am. Chem. Soc. 130 (2008) 1085–1092.
[68] S.L. Yau, Y.G. Kim, K. Itaya, J. Phys. Chem. B 101 (1997) 3547–3553.
[69] J.R. Gong, L.J. Wan, Q.H. Yuan, C.L. Bai, H. Jude, P.J. Stang, Proc. Natl. Acad. Sci. U.S.A. 102 (2005) 971–974.
[70] T. Kudernac, N. Sandig, T.F. Landaluce, B.J. van Wees, P. Rudolf, N. Katsonis, F. Zerbetto, B.L. Feringa, J. Am. Chem. Soc. 131 (2009) 15655–15659.
[71] Y.L. Yang, C. Wang, Curr. Opin. Colloid Interface Sci. 14 (2009) 135–147.
[72] X. Shao, X.C. Luo, X.Q. Hu, K. Wu, J. Phys. Chem. B 110 (2006) 1288–1293.
[73] B.J. Gyarfas, B. Wiggins, M. Zosel, K.W. Hipps, Langmuir 21 (2005) 919–923.
[74] M. Lackinger, S. Griessl, W.A. Heckl, M. Hietschold, G.W. Flynn, Langmuir 21 (2005) 4984–4988.
[75] L. Kampschulte, M. Lackinger, A.K. Maier, R.S.K. Kishore, S. Griessl, M. Schmittel, W.M. Heckl, J. Phys. Chem. B 110 (2006) 10829–10836.
[76] T. Chen, D. Wang, X. Zhang, Q.L. Zhou, R.B. Zhang, L.J. Wan, J. Phys. Chem. C 114 (2010) 533–538.
[77] J. Elemans, I. De Cat, H. Xu, S. De Feyter, Chem. Soc. Rev. 38 (2009) 722–736.
[78] R. Yamada, K. Uosaki, Langmuir 13 (1997) 5218–5221.
[79] R. Yamada, K. Uosaki, Langmuir 14 (1998) 855–861.
[80] S.S. Li, L.P. Xu, L.J. Wan, S.T. Wang, L. Jiang, J. Phys. Chem. B 110 (2006) 1794–1799.
[81] X. Zhang, T. Chen, Q. Chen, G.J. Deng, Q.H. Fan, L.J. Wan, Chem. Eur. J. 15 (2009) 9669–9673.
[82] S.B. Lei, K. Tahara, F.C. De Schryver, M. Van der Auweraer, Y. Tobe, S. De Feyter, Angew. Chem. Int. Ed. 47 (2008) 2964–2968.
[83] M. Stohr, M. Wahl, C.H. Galka, T. Riehm, T.A. Jung, L.H. Gade, Angew. Chem. Int. Ed. 44 (2005) 7394–7398.
[84] G.J.J. Su, R. Aguilar-Sanchez, Z.H. Li, I. Pobelov, M. Homberger, U. Simon, T. Wandlowski, ChemPhysChem 8 (2007) 1037–1048.
[85] C.J. Li, Q.D. Zeng, Y.H. Liu, L.J. Wan, C. Wang, C.R. Wang, C.L. Bai, ChemPhysChem 4 (2003) 857–859.
[86] D. Rohde, C.J. Yan, H.J. Yan, L.J. Wan, Angew. Chem. Int. Ed. 45 (2006) 3996–4000.
[87] D. Wang, Q. Chen, L.J. Wan, Phys. Chem. Chem. Phys. 10 (2008) 6467–6478.
[88] S. De Feyter, J. Hofkens, M. Van der Auweraer, R.J.M. Nolte, K. Mullen, F.C. De Schryver, Chem. Commun. (2001) 585–592.
[89] M.J. Comstock, N. Levy, A. Kirakosian, J.W. Cho, F. Lauterwasser, J.H. Harvey, D.A. Strubbe, J.M.J. Frechet, D. Trauner, S.G. Louie, M.F. Crommie, Phys. Rev. Lett. 99 (2007).
[90] P. Vanoppen, P.C.M. Grim, M. Rucker, S. DeFeyter, G. Moessner, S. Valiyaveettil, K. Mullen, F.C. DeSchryver, J. Phys. Chem. 100 (1996) 19636–19641.
[91] L.P. Xu, L.J. Wan, J. Phys. Chem. B 110 (2006) 3185–3188.
[92] N. Katsonis, T. Kudernac, M. Walko, S.J. van der Molen, B.J. van Wees, B.L. Feringa, Adv. Mater. 18 (2006) 1397.
[93] L.P. Xu, C.J. Yan, L.J. Wan, S.G. Jiang, M.H. Liu, J. Phys. Chem. B 109 (2005) 14773–14778.
[94] M.M.S. Abdel-Mottaleb, S. De Feyter, A. Gesquiere, M. Sieffert, M. Klapper, K. Mullen, F.C. De Schryver, Nano Lett. 1 (2001) 353–359.
[95] C.S. Tsai, J.K. Wang, R.T. Skodje, A.C. Lin, J. Am. Chem. Soc. 127 (2005) 10788–10789.
[96] Y.H. Qiao, Q.D. Zeng, Z.Y. Tan, S.D. Xu, D. Wang, C. Wang, L.J. Wan, C.L. Bai, J. Vac. Sci. Technol. B 20 (2002) 2466–2469.
[97] Y. Okawa, M. Aono, Surf. Sci. 514 (2002) 41–47.
[98] A. Miura, S. De Feyter, M.M.S. Abdel-Mottaleb, A. Gesquiere, P.C.M. Grim, G. Moessner, M. Sieffert, M. Klapper, K. Mullen, F.C. De Schryver, Langmuir 19 (2003) 6474–6482.
[99] Y. Okawa, M. Aono, Nature 409 (2001) 683–684.
[100] G. Pace, V. Ferri, C. Grave, M. Elbing, C. von Hanisch, M. Zharnikov, M. Mayor, M.A. Rampi, P. Samori, Proc. Natl. Acad. Sci. U.S.A. 104 (2007) 9937–9942.
[101] D.M. Kolb, Angew. Chem. Int. Ed. 40 (2001) 1162–1181.
[102] D. Wang, L.J. Wan, J. Phys. Chem. C 111 (2007) 16109–16130.
[103] W.B. Cai, L.J. Wan, H. Noda, Y. Hibino, K. Ataka, M. Osawa, Langmuir 14 (1998) 6992–6998.
[104] L.J. Wan, H. Noda, C. Wang, C.L. Bai, M. Osawa, ChemPhysChem 2 (2001) 617–619.
[105] T. Dretschkow, D. Lampner, T. Wandlowski, J. Electroanal. Chem. 458 (1998) 121–138.
[106] Y.X. Diao, M.J. Han, L.J. Wan, K. Itaya, T. Uchida, H. Miyake, A. Yamakata, M. Osawa, Langmuir 22 (2006) 3640–3646.
[107] D. Mayer, T. Dretschkow, K. Ataka, T. Wandlowski, J. Electroanal. Chem. 524 (2002) 20–35.
[108] G.J. Su, H.M. Zhang, L.J. Wan, C.L. Bai, T. Wandlowski, J. Phys. Chem. B 108 (2004) 1931–1937.
[109] Z. Li, B. Han, L.J. Wan, T. Wandlowski, Langmuir 21 (2005) 6915–6928.
[110] R. Wen, G.B. Pan, U.J. Wan, J. Am. Chem. Soc. 130 (2008) 12123–12127.
[111] H. Sakaguchi, H. Matsumura, H. Gong, A.M. Abouelwafa, Science 310 (2005) 1002–1006.
[112] H. Sakaguchi, H. Matsumura, H. Gong, Nat. Mater. 3 (2004) 551–557.
[113] J.D. Mougous, A.J. Brackley, K. Foland, R.T. Baker, D.L. Patrick, Phys. Rev. Lett. 84 (2000) 2742–2745.
[114] A.M. Berg, D.L. Patrick, Angew. Chem. Int. Ed. 44 (2005) 1821–1823.
[115] S.B. Lei, S.X. Yin, C. Wang, L.J. Wan, C.L. Bai, Chem. Mater. 14 (2002) 2837.
[116] S.B. Lei, C. Wang, S.X. Yin, C.L. Bai, J. Phys. Chem. B 105 (2001) 12272–12277.
[117] S. Yoshimoto, K. Itaya, J. Porphyrins Phthalocyanines 11 (2007) 313–333.
[118] K. Suto, S. Yoshimoto, K. Itaya, J. Am. Chem. Soc. 125 (2003) 14976–14977.
[119] K. Suto, S. Yoshimoto, K. Itaya, Langmuir 22 (2006) 10766–10776.
[120] L. Wang, Q. Chen, G.B. Pan, L.J. Wan, S.M. Zhang, X.W. Zhan, B.H. Northrop, P.J. Stang, J. Am. Chem. Soc. 130 (2008) 13433–13441.
[121] J.R. Gong, H.J. Yan, Q.H. Yuan, L.P. Xu, Z.S. Bo, L.J. Wan, J. Am. Chem. Soc. 128 (2006) 12384–12385.
[122] Y.B. Li, Z. Ma, K. Deng, S.B. Lei, Q.D. Zeng, X.L. Fan, S. De Feyter, W. Huang, C. Wang, Chem. Eur. J. 15 (2009) 5418–5423.
[123] J. Adisoejoso, K. Tahara, S. Okuhata, S. Lei, Y. Tobe, S. De Feyter, Angew. Chem. Int. Ed. 48 (2009) 7353–7357.
[124] G.B. Pan, L.J. Wan, Q.Y. Zheng, C.L. Bai, Chem. Phys. Lett. 367 (2003) 711–716.
[125] G.B. Pan, J.H. Bu, D. Wang, J.M. Liu, L.J. Wan, Q.Y. Zheng, C.L. Bai, J. Phys. Chem. B 107 (2003) 13111–13116.
[126] S. Yoshimoto, M. Abe, K. Itaya, F. Narumi, K. Sashikata, K. Nishiyama, I. Taniguchi, Langmuir 19 (2003) 8130–8133.
[127] G.J. Su, L.H. Gan, Z.Y. Yang, G.B. Pan, L.J. Wan, C.R. Wang, J. Phys. Chem. B 110 (2006) 5559–5562.
[128] G.B. Pan, J.M. Liu, H.M. Zhang, L.J. Wan, Q.Y. Zheng, C.L. Bai, Angew. Chem. Int. Ed. 42 (2003) 2747–2751.
[129] T. Kudernac, S.B. Lei, J.A.A.W. Elemans, S. De Feyter, Chem. Soc. Rev. 38 (2009) 3505.
[130] A. Langner, S.L. Tait, N. Lin, C. Rajadurai, M. Ruben, K. Kern, Proc. Natl. Acad. Sci. U.S.A. 104 (2007) 17927–17930.
[131] U. Schlickum, R. Decker, F. Klappenberger, G. Zoppellaro, S. Klyatskaya, M. Ruben, I. Silanes, A. Arnau, K. Kern, H. Brune, J.V. Barth, Nano Lett. 7 (2007) 3813–3817.
[132] S. Stepanow, M. Lingenfelder, A. Dmitriev, H. Spillmann, E. Delvigne, N. Lin, X.B. Deng, C.Z. Cai, J.V. Barth, K. Kern, Nat. Mater. 3 (2004) 229–233.
[133] R. Madueno, M.T. Raisanen, C. Silien, M. Buck, Nature 454 (2008) 618–621.
[134] H. Zhou, H. Dang, J.H. Yi, A. Nanci, A. Rochefort, J.D. Wuest, J. Am. Chem. Soc. 129 (2007) 13774.
[135] Z. Ma, Y.Y. Wang, P. Wang, W. Huang, Y.B. Li, S.B. Lei, Y.L. Yang, X.L. Fan, C. Wang, ACS Nano 1 (2007) 160–167.
[136] K. Tahara, C.A. Johnson, T. Fujita, M. Sonoda, F.C. De Schryver, S. De Feyter, M.M. Haley, Y. Tobe, Langmuir 23 (2007) 10190–10197.
[137] K. Tahara, S. Furukawa, H. Uji-I, T. Uchino, T. Ichikawa, J. Zhang, W. Mamdouh, M. Sonoda, F.C. De Schryver, S. De Feyter, Y. Tobe, J. Am. Chem. Soc. 128 (2006) 16613–16625.

[138] G. Schull, L. Douillard, C. Fiorini-Debuisschert, F. Charra, F. Mathevet, D. Kreher, A.J. Attias, Nano Lett. 6 (2006) 1360–1363.
[139] J. Lu, S.B. Lei, Q.D. Zeng, S.Z. Kang, C. Wang, L.J. Wan, C.L. Bai, J. Phys. Chem. B 108 (2004) 5161–5165.
[140] X.H. Kong, K. Deng, Y.L. Yang, Q.D. Zeng, C. Wang, J. Phys. Chem. C 111 (2007) 17382–17387.
[141] S.S. Li, H.J. Yan, L.J. Wan, H.B. Yang, B.H. Northrop, P.J. Stang, J. Am. Chem. Soc. 129 (2007) 9268–9269.
[142] X.H. Kong, K. Deng, Y.L. Yang, Q.D. Zeng, C. Wang, J. Phys. Chem. C 111 (2007) 9235–9239.
[143] Y.H. Liu, S.X. Yin, C.C. Ma, G.H. Chen, C. Wang, L.J. Wan, C.L. Bai, Surf. Sci. 559 (2004) 40–46.
[144] J. Lu, Q.D. Zeng, C. Wang, L.J. Wan, C.L. Bai, Chem. Lett. 32 (2003) 856–857.
[145] M.M.S. Abdel-Mottaleb, E. Gomar-Nadal, M. Surin, H. Uji-i, W. Mamdouh, J. Veciana, V. Lemaur, C. Rovira, J. Cornil, R. Lazzaroni, D.B. Amabilino, S. De Feyter, F.C. De Schryver, J. Mater. Chem. 15 (2005) 4601–4615.
[146] J. Otsuki, S. Kawaguchi, T. Yamakawa, M. Asakawa, K. Miyake, Langmuir 22 (2006) 5708–5715.
[147] S. Yoshimoto, T. Sawaguchi, W. Su, J.Z. Jiang, N. Kobayashi, Angew. Chem. Int. Ed. 46 (2007) 1071–1074.
[148] S. Yoshimoto, E. Tsutsumi, Y. Honda, Y. Murata, M. Murata, K. Komatsu, O. Ito, K. Itaya, Angew. Chem. Int. Ed. 43 (2004) 3044–3047.
[149] S. Yoshimoto, Y. Honda, Y. Murata, M. Murata, K. Komatsu, O. Ito, K. Itaya, J. Phys. Chem. B 109 (2005) 8547–8550.
[150] S. Yoshimoto, A. Saito, E. Tsutsumi, F. D'Souza, O. Ito, K. Itaya, Langmuir 20 (2004) 11046–11052.
[151] S.B. Lei, C. Wang, X.L. Fan, L.J. Wan, C.L. Bai, Langmuir 19 (2003) 9759–9763.
[152] S. Hoeppener, L.F. Chi, H. Fuchs, ChemPhysChem 4 (2003) 494–498.
[153] M.M.S. Abdel-Mottaleb, N. Schuurmans, S. De Feyter, J. Van Esch, B.L. Feringa, F.C. De Schryver, Chem. Commun. (2002) 1894–1895.
[154] S.B. Lei, K. Tahara, X.L. Feng, S.H. Furukawa, F.C. De Schryver, K. Mullen, Y. Tobe, S. De Feyter, J. Am. Chem. Soc. 130 (2008) 7119–7129.